

Accuracy of macroscopic and microscopic pK_a predictions of small molecules evaluated by the SAMPL6 Blind Challenge

Mehtap Isik (ORCID: [0000-0002-6789-952X](#))^{1,2*}, Ariën S. Rustenburg (ORCID: [0000-0002-3422-0613](#))^{1,3}, Andrea Rizzi (ORCID: [0000-0001-7693-2013](#))^{1,4}, M. R. Gunner⁶, David L. Mobley (ORCID: [0000-0002-1083-5533](#))⁵, John D. Chodera (ORCID: [0000-0003-0542-119X](#))¹

¹Computational and Systems Biology Program, Sloan Kettering Institute, Memorial Sloan Kettering Cancer Center, New York, NY 10065, United States; ²Tri-Institutional PhD Program in Chemical Biology, Weill Cornell Graduate School of Medical Sciences, Cornell University, New York, NY 10065, United States; ³Graduate Program in Physiology, Biophysics, and Systems Biology, Weill Cornell Medical College, New York, NY 10065, United States; ⁴Tri-Institutional PhD Program in Computational Biology and Medicine, Weill Cornell Graduate School of Medical Sciences, Cornell University, New York, NY 10065, United States; ⁵Department of Pharmaceutical Sciences and Department of Chemistry, University of California, Irvine, Irvine, California 92697, United States; ⁶Department of Physics, City College of New York, New York NY 10031

*For correspondence:
mehtap.isik@choderlab.org (MI)

17

Abstract

Acid dissociation constant (pK_a) prediction is a prerequisite for predicting many other properties of small molecules such as protein-ligand binding affinity, distribution coefficient ($\log D$), membrane permeability, and solubility due to the necessity of predicting relevant protonation states and the free energy penalty of each state. SAMPL6 pK_a Challenge was the first time that a separate challenge was conducted for evaluating pK_a predictions as a part of SAMPL. It was motivated by the inaccuracies observed in prior physical property prediction challenges, such as SAMPL5 $\log D$ Challenge, caused by protonation state and pK_a prediction issues. The goal of the pK_a challenge was to elucidate the performance of contemporary pK_a prediction methods for drug-like molecules. The challenge set was composed of 24 kinase inhibitor fragment-like small molecules and some of them were multiprotic. 11 research groups contributed blind prediction sets of 37 pK_a prediction methods. Four widely used pK_a prediction methods that were missing from blind predictions were added as reference methods to challenge analysis. Collecting both microscopic and macroscopic pK_a predictions allowed in-depth evaluation of pK_a prediction performance. This article highlights deficiencies of typical pK_a prediction evaluation approaches when the difference between microscopic and macroscopic pK_a s is ignored and suggests more stringent evaluation criteria for microscopic and macroscopic pK_a predictions guided by the available experimental data. Top-performing submissions for macroscopic pK_a predictions achieved RMSE of 0.7-1.0 units and included both quantum-mechanical and empirical approaches. These predictions included less than 8 extra/missing macroscopic pK_a s for the set of 24 molecules. A large number of submissions had RMSE spanning 1-3 pK_a units. Molecules with sulfur-containing heterocycles, iodo, and bromo groups suffered from less accurate pK_a predictions on average considering all methods evaluated. For a subset of molecules, the available NMR-based dominant microstate sequence data was utilized to elucidate dominant tautomer prediction errors of microscopic pK_a predictions which was prominent for charged tautomers. SAMPL6 pK_a Challenge demonstrated the need for improving pK_a prediction methods for drug-like molecules, especially for challenging moieties and multiprotic molecules. The level of pK_a prediction inaccuracy observed in this challenge has potential to be detrimental to the performance of protein-ligand binding affinity predictions in two ways: (1) errors in predicted dominant charge and tautomeric state and (2) errors in the calculation of free energy correction for minor and multiple protonation states of the ligand.

43 0.1 Keywords

44 SAMPL · blind prediction challenge · acid dissociation constant · pK_a · small molecule · macroscopic pK_a · microscopic pK_a · macro-
45 scopic protonation state · microscopic protonation state

46 0.2 Abbreviations

47 **SAMPL** Statistical Assessment of the Modeling of Proteins and Ligands

48 **pK_a** $-\log_{10}$ acid dissociation equilibrium constant

49 **SEM** Standard error of the mean

50 **RMSE** Root mean squared error

51 **MAE** Mean absolute error

52 τ Kendall's rank correlation coefficient (Tau)

53 **R²** Coefficient of determination (R-Squared)

54 1 Introduction

55 The acid dissociation constant (pK_a) describes the protonation state equilibrium of a molecule given pH. Predicting pK_a is a
56 prerequisite for predicting many other properties of small molecules such as protein-ligand binding affinity, distribution coeffi-
57 cient ($\log D$), membrane permeability, and solubility. Computer-aided drug design efforts include assessing properties of virtual
58 molecules to guide synthesis and prioritization decisions. In such cases an experimental pK_a measurement is not possible.
59 Therefore, accurate computational pK_a prediction methods are required.

60 For a monoprotic weak acid (HA) or base (B) dissociation equilibria shown in Equation 1, the acid dissociation constant is
61 expressed as in Equations 2 or its common negative logarithmic form as in Equation 3. The ratio of ionization states can be
62 calculate with HHenderson-Hasselbalch equations shown in Equation 4.



$$K_a = \frac{[A^-][H^+]}{[HA]} \quad K_a = \frac{[B][H^+]}{[BH^+]} \quad (2)$$

$$pK_a = -\log_{10} K_a \quad (3)$$

$$pH = pK_a + \log_{10} \frac{[A^-]}{[HA]} \quad pH = pK_a + \log_{10} \frac{[B]}{[BH^+]} \quad (4)$$

63 Ionizable sites are found often in drug molecules and influence their pharmaceutical properties including target affinity,
64 ADME/Tox, and formulation properties [1]. Drug molecules with titratable groups can exist in many different charge and proto-
65 nation states based on the pH of the environment. We rely on pK_a values to determine in which charge and protonation states
66 the molecules exists and relative populations of these states. The pH of the human gut ranges between 1-8 and 74% of approved
67 drugs can change ionization states withing this physiological pH range [2] and because of this pK_a values of drug molecules pro-
68 vides essential information about their physicochemical and pharmaceutical properties. A wide distribution of acidic and basic
69 pK_a values, ranging from 0 to 12, have been observed in approved drugs [1, 2].

70 Small molecule pK_a predictions influence computational protein-ligand binding affinities in multiple ways. Errors in pK_a pre-
71 dictions can cause modeling the wrong charge, protonation, and tautomerization states which affect hydrogen bonding oppor-
72 tunities and charge distribution of the ligand. The prediction of the dominant protonation state and relative population of minor
73 states in aqueous medium is dictated by the pK_a values. The relative free energy of different protonation states in the aque-
74 ous state is a function of pK_a and pH, it contributes to the overall protein-ligand affinity in the form of a free energy penalty of
75 reaching higher energy protonation states [3].

76 Drug-like molecules present difficulties for pK_a prediction compared to simple monoprotic molecules. Drug-like molecules
77 are frequently multiprotic, have large conjugated systems, heterocycles, tautomerization. In addition that larger molecules
78 with conformational flexibility can have intramolecular hydrogen bonding which shifts pK_a values. These shifts could be real or

79 modeling artifacts due to collapsed conformations caused by deficiencies in solvation models. Yet predicting pK_a s of drug-like
80 molecules accurately is a prerequisite for computational drug discovery and design.

81 The definition of pK_a diverges into two for multiprotic molecules: macroscopic pK_a and microscopic pK_a [4–6]. Macroscopic
82 pK_a describes the equilibrium dissociation constant between different charged states of the molecule. Each charge state can be
83 composed of multiple tautomers. Macroscopic pK_a is about the deprotonation of the molecule, not a particular titratable group.
84 Microscopic pK_a describes the acid dissociation equilibrium between individual tautomeric states of different charges. We refer
85 to collection of all tautomeric states of different macroscopic states (charge states) as microscopic states. Microscopic pK_a value
86 defined between two microstates captures the deprotonation of a single titratable group with a fixed background protonation
87 state of other titratable groups. In molecules with multiple titratable groups, the protonation state of one group can affect the
88 proton dissociation propensity of another functional group, therefore the same titratable group may have different microscopic
89 pK_a values based on the protonation state of the rest of the molecule. Different experimental methods capture different def-
90 initions of pK_a s as explained in more detail in this prior publication [7]. Most common pK_a measurement techniques such as
91 potentiometric and spectrophotometric methods measure macroscopic pK_a s while NMR measurements can determine micro-
92 scopic pK_a s and microstate populations. Therefore, it is important to pay attention to the source and definition of pK_a values
93 to interpret their meaning correctly. Computational methods can predict both microscopic and macroscopic pK_a s. While micro-
94 scopic pK_a predictions are more informative for determining relevant microstates/tautomers of a molecule and their relative
95 free energies, computing predicted macroscopic pK_a s is useful for direct comparison of methods to more common macroscopic
96 experimental measurements. In this paper, we explore approaches to assess the performance of both macroscopic and micro-
97 scopic pK_a predictions, taking advantage of available experimental data.

98 Microscopic pK_a predictions can be converted to macroscopic pK_a predictions either directly with the equation 5 [?] or
99 through computing the macroscopic free energy of deprotonation between ionization states with charges N and N-1 via Boltz-
100 mann weighted sum of the relative free energy of microstates (G_i) as in equations 6 and 7 [8].

$$K_a^{\text{macro}} = \sum_{j=1}^{N_{\text{deprot}}} \frac{1}{\sum_{i=1}^{N_{\text{prot}}} \frac{1}{K_{ij}^{\text{micro}}}} , \quad (5)$$

$$\Delta G_{N-1,N} = RT \ln \frac{\sum_i e^{-G_i/RT} \delta_{N_i, N-1}}{\sum_i e^{-G_i/RT} \delta_{N_i, N}} \quad (6)$$

$$pK_a = pH - \frac{\Delta G_{N-1,N}}{RT \ln 10} \quad (7)$$

101 In Equation 6 $\Delta G_{N-1,N}$ is the effective macroscopic protonation free energy. $\delta_{N_i, N-1}$ is equal to 1 when the microstate i has a
102 total charge of N-1 and null otherwise. $\delta_{N_i, N}$ is equal to 1 when the microstate i has a total charge of N and null otherwise. RT is
103 the ideal gas constant times the temperature.

104 1.1 Motivation for a blind pK_a challenge

105 SAMPL (Statistical Assessment of the Modeling of Proteins and Ligands) is a series of annual computational prediction chal-
106 lenges for the computational chemistry community. The goal of SAMPL is evaluate to current performance of the models and to
107 bring the attention of quantitative biomolecular modeling field on major issues that limit the accuracy of protein-ligand binding
108 models.

109 SAMPL Challenges that focus on different physical properties so far have assessed intermolecular binding models of various
110 protein-ligand and host-guest systems, solvation models to predict hydration free energies and distribution coefficients. Poten-
111 tial benefits of these challenges are motivating improvement computational methods and revealing unexpected contributors to
112 error by focusing on interesting test systems. SAMPL Challenges have demonstrated the effects of force field accuracy, sampling
113 issues, solvation modeling defects, and tautomer/protonation state predictions on protein-ligand binding predictions.

114 During the SAMPL5 log D Challenge, the performance of cyclohexane-water log D predictions were lower than expected and
115 accuracy suffered when protonation states and tautomers were not taken into account [9, 10]. With the motivation of decon-
116 voluting the different sources of error contributing to the large errors observed in the SAMPL5 log D Challenge, we organized

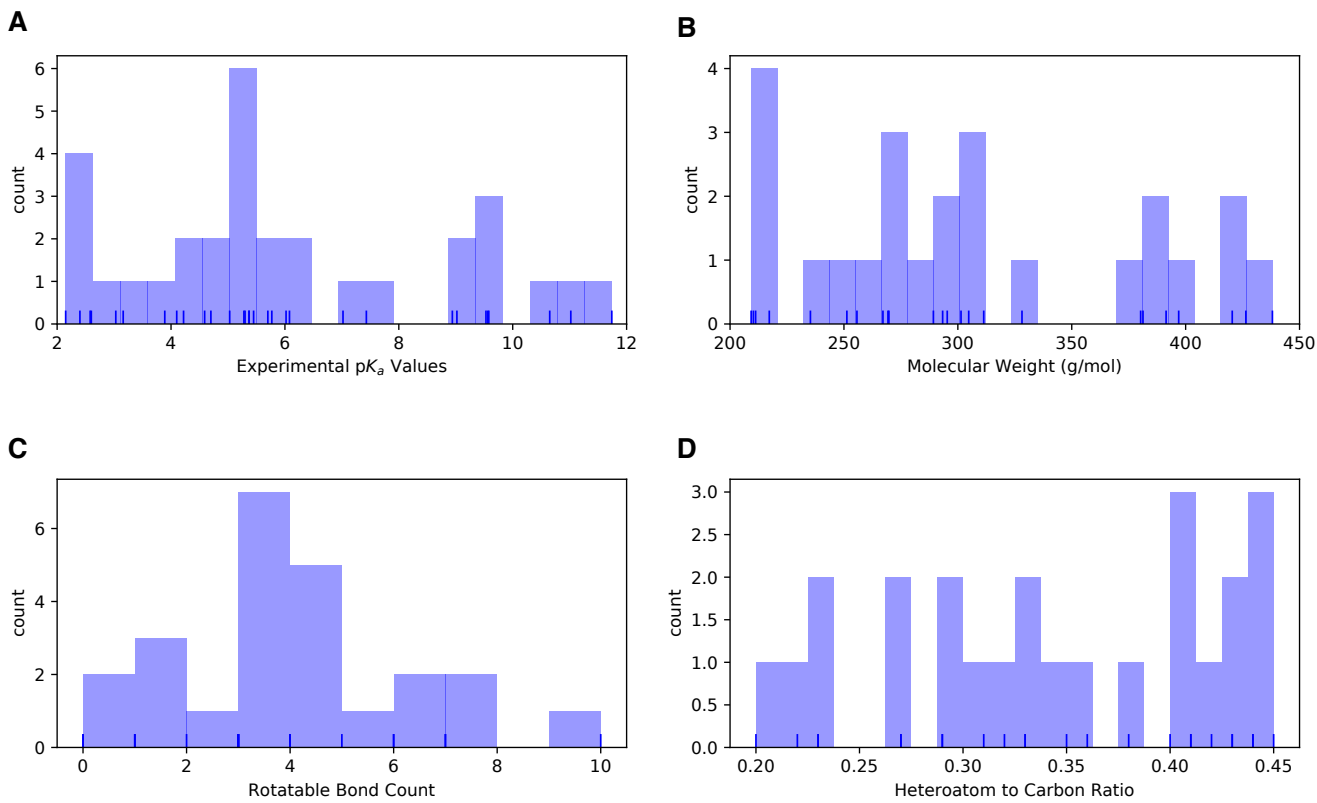


Figure 1. Distribution of molecular properties of 24 compounds in SAMPL6 pK_a Challenge. **A** Histogram of spectrophotometric pK_a measurements collected with Sirius T3 [7]. Overlayed carpet plot indicates the actual values. Five compounds have multiple measured pK_a s in the range of 2-12. **B** Histogram of molecular weights of compounds in SAMPL6 set. Molecular weights were calculated by neglecting counter ions. **C** Histogram of the number of non-terminal rotatable bonds in each molecule. **D** The histogram of the ratio of heteroatom (non-carbon heavy atom) count to the number of carbon atoms.

separate of pK_a and $\log P$ challenges in SAMPL6 [7, 11, 12]. For this iteration of the SAMPL challenge, we have taken one step back and isolated just the problem of predicting aqueous protonation states.

This is the first time a blind pK_a prediction challenge has been fielded as part of SAMPL. In this first iteration of the challenge, we aimed to assess the performance of current pK_a prediction methods for drug-like molecules, investigate potential causes of inaccurate pK_a estimates, and determine how much current level of expected accuracy might impact protein binding affinity predictions. In binding free energy predictions, any error in predicting the free energy of accessing a minor aqueous protonation state of ligand that contributes to the complex formation will directly add to the error in the predicted binding free energy. Similarly for $\log D$ predictions, inaccurate prediction aqueous protonation state that contribute partitioning between phases or prediction of relative free energy of these states will be detrimental to the accuracy of transfer free energy predictions.

1.2 Approaches to predict small molecule pK_a s

Overview of kinds of pK_a prediction methods available. Define method categories: DL, LFER, QSPR/ML, QM, QM+LEC, and QM+MM

128 2 Methods

129 2.1 Design and logistics of the SAMPL6 pK_a Challenge

The SAMPL6 pK_a Challenge was conducted as a blind prediction challenge focus on predicting aqueous pK_a value of 24 small molecules that resemble fragments of kinase inhibitors. The compound selection process was described in depth in the prior

132 publication reporting SAMPL6 pK_a Challenge experimental data collection [7]. The distribution of molecular weights, experimen-
133 tal pK_a values, number of rotatable bonds, and heteroatom to carbon ratio are depicted in Fig. 1. The challenge molecule set
134 was composed of 17 small molecules with limited flexibility (less than 5 non-terminal rotatable bonds) and 7 molecules with
135 5-10 non-terminal rotatable bonds. The distribution of experimental pK_a values ranged between 2-12 and roughly uniform. 2D
136 representations of all compounds were provided in Fig. 5. Drug-like molecules are often larger and more complex than the ones
137 used in this study, however, aimed for the

138 The dataset composition and details of the pK_a measurement technique, except the identity of the small molecules, were
139 announced about a month before the challenge start time. Experimental macroscopic pK_a measurements were collected with
140 spectrophotometric method of Sirius T3, at room temperature in ionic strength-adjusted water with 0.15 M KCl [7]. The instruc-
141 tions for participation and the identity of the challenge molecules were released at the challenge start date (October 25, 2017).
142 A table of molecule IDs (in the form of SM##) and their canonical isomeric SMILES was provided as input. Blind prediction
143 submissions were accepted until January 22, 2018.

144 Following the conclusion of the blind challenge, the experimental data was made public on January 23, 2018. The SAMPL
145 organizers and participants gathered at the Second Joint D3R/SAMPL Workshop, at UC San Diego, La Jolla, CA on February 22-23,
146 2018 to share results. The workshop aimed to create an opportunity for participants to have discussions, evaluate the results
147 and lessons of the challenge together. The participants reported their results and their own evaluations in the special issue of
148 the Journal of Computer-Aided Molecular Design [13].

149 In this first iteration of pK_a prediction challenge we were not sure what was the best way to capture all necessary informa-
150 tion related to pK_a predictions. Our aim was to directly evaluate macroscopic pK_a predictions comparing them to experimental
151 macroscopic pK_a values and to use collected microscopic pK_a prediction data for more in-depth diagnostics of method perfor-
152 mance. Therefore, we asked participants to submit their predictions in three different submission types:

- 153 • **Type I:** microscopic pK_a values and related microstate pairs
- 154 • **Type II:** fractional microstate populations as a function of pH in 0.1 pH increments
- 155 • **Type III:** macroscopic pK_a values

156 For each submission type, a machine-readable submission file template was specified. For type I submissions, participants
157 were asked to report microstate ID of protonated state, microstate ID of deprotonated state, microscopic pK_a, microscopic
158 pK_a SEM. The reason and method of microstate enumeration is discussed further in Section 2.2 "Enumeration of Microstates".
159 The SEM captures the statistical uncertainty of the predicted method. Microstate IDs were preassigned identifiers for each mi-
160 crostates in the form of SM##_micro##. For type II submission, submission format included a table that started with microstate
161 ID and consecutive columns reporting natural logarithm of fractional microstate population values of each predicted microstate
162 for 0.1 pH increments between pH 2 and 12. For type III submissions participants were asked to report molecule ID, macroscopic
163 pK_a, macroscopic pK_a SEM. It was mandatory to submit predictions for all fields for each prediction, but it was not mandatory to
164 submit predictions for all the molecules or all the submission types. Although we have accepted submissions with partial sets of
165 molecules, it would have been a better choice to require predictions for all the molecules for better comparison of method per-
166 formance. The submission files also included fields for naming the method, listing the software utilized, and a free text method
167 section for the detailed documentation of each method.

168 Participants were allowed to submit predictions with multiple methods as long as they create separate submissions files.
169 Anonymous participation to the challenge was allowed, however all participant opted to make their submissions public. All blind
170 submissions were assigned a unique 5-digit alphanumeric submission ID, which will be used throughout this paper. Unique IDs
171 were also assigned when multiple submissions exists for different submission types of the same method such as microscopic
172 pK_a(type I) and macroscopic pK_a (type III). These submission IDs were also reported in the evaluation papers of participants and
173 allow cross-referencing. Submission IDs, participant provided method names, and method categories are presented in Table 1.
174 There were many instances that multiple types of submissions of the same method were provided by participants as challenge
175 instructions requested. Although each prediction set was assigned a separate submission ID we have matched the submissions
176 that originated from the same method according to the reports of the participant. Submission ID for both macroscopic (type III)
177 and microscopic (type I) pK_a predictions of each method (when exists) are shown in Table 1.

178 2.2 Enumeration of microstates

179 To capture both the pK_a value and titration position of microscopic pK_a predictions, we needed microscopic pK_a predictions to
180 be reported together with the pair of deprotonated and protonated microstates that describes the transition. String represen-

tations of molecules such as canonical SMILES with explicit hydrogens can be written, however, there can be inconsistencies between the interpretation of canonical SMILES written by different softwares and algorithms. In order to avoid complications while reading microstate structure files from different sources, we have decided that the safest route was pre-enumerating all possible microstates of challenge compounds, assigning the microstates IDs to each in the form of SM##_micro##, and require participants to report microstate pairs using the provided microstates IDs.

We enumerated an initial list of microstates with Epik and OpenEye QUACPAC and took the union of results. Microstates with Epik were generated using Schrodinger Suite v2016-4, and running Epik to enumerate all tautomers within 20 pK_a units of pH 7. For enumerating microstates with OpenEye QUACPAC, we had to first enumerate formal charges and for each charge enumerate all possible tautomers using the settings of maximum tautomer count 200, level 5, and carbonyl hybridization False. Then we created an union of all enumerated states written as canonical isomeric SMILES. Even though resonance structures correspond to different canonical isomeric SMILES they are not different microstates, therefore it was necessary to remove resonance structures that were replicates of the same tautomer. To detect resonance structures we converted canonical isomeric SMILES to InChI hashes with explicit and fixed hydrogen layer. Structures that describe the same tautomer but different resonance states lead to explicit hydrogen InChI hashes that are identical allowing replicates to be removed. The Jupyter Notebook used for the enumeration of microstates is provided in supplementary documents. Because resonance and geometric isomerism should be ignored when matching predicted structures microstate IDs (except SM20 which should be modelled as E-isomer), we provided microstate ID tables with canonical SMILES and 2D-depictions.

Despite pooling together enumerated charge states and tautomers with Epik and OpenEye QUACPAC to our surprise the microstate lists were still incomplete. A better algorithm that can enumerate all possible microstates would be very beneficial. In SAMPL6 Challenge participants came up with new microstates that were not present in the initial list that we provided. Based on participant requests we iteratively had to update the list of microstates and assign new microstate IDs. Every time we received a request, we shared the updated microstate ID lists with all the challenge participants.

A working pK_a microstate definition for this challenge was provided in challenge instructions for clarity. Physically meaningful microscopic pK_a s are defined between microstate pairs that can interconvert by single protonation/deprotonation event of only one titratable group. So, microstate pairs should have total charge difference of |1| and only one heavy atom that differs in the number of bound hydrogens, regardless of resonance state or geometric isomerism. All geometric isomer and resonance structure pairs that have the same number of hydrogens bound to equivalent heavy atoms are related to the same microstate. Pairs of resonance structures and geometric isomers (cis/trans, stereo) won't be considered as different microstates, as long as there is no change in the number of hydrogens bound to each heavy atom in these structures. Since we wanted to participants to report only microscopic pK_a s that are describe single deprotonation events (in contrast to transitions between microstates that are different in terms of two or more titratable protons), we have also provided a pre-enumerated list of allowed microstate pairs.

Provided microstate ID and microstate pair lists were intended to be used for reporting microstate IDs and to aid parsing of submissions. The enumerated lists of microstates were not created with the intent to guide computational predictions. This was clearly stated in the challenge instructions. However, we noticed that some participants still used the microstate lists as an input for their pK_a predictions as we received complaints from participants that due to our updates to microstate lists they needed to repeat their calculations. This would not have been an issue, if participants used pK_a prediction protocols that did not rely on an external pre-enumerated list of microstates as an input. None of the participants have reported this dependency in their method descriptions explicitly, therefore we can not identify which submissions have used the enumerated microstate lists as input and which ones has followed the instructions.

2.3 Evaluation approaches

Since the experimental data for the challenge was mainly composed of macroscopic pK_a values of both monoprotic and multi-protic compounds, evaluation of macroscopic and microscopic pK_a predictions was not straightforward. For only a subset of 8 molecules, dominant microstate sequence could be inferred from NMR. For the rest of the molecules the only experimental information available was the macroscopic pK_a value, while experimental data did not provide any information on which group(s) are being titrated, microscopic pK_a values, identity of associated macrostates (which charge) or microstates (which tautomers). In this comparative performance evaluation of we let the experimental data lead the challenge analysis towards various evaluation routes. To compare macroscopic pK_a predictions to experimental values we had to utilize numerical matching algorithms before we could calculate performance statistics. For the subset of molecules with experimental data about microstates, we used microstate based matching. These matching methods were described further in the next section.

231 Three types of submissions were collected during the SAMPL6 pK_a Challenge. We have only utilized type I (microscopic pK_a
232 value and microstate IDs) and type III (macroscopic pK_a value) predictions in this article. Type I submissions contained the same
233 prediction information as the the type II submissions which reported fractional population of microstates with respect to pH.

234 2.3.1 Matching algorithms for pairing predicted and experimental pK_a s

235 Macroscopic pK_a predictions can be calculated from microscopic pK_a s for direct comparison to experimental macroscopic pK_a
236 values, although there is still a remaining issue. How to match predicted macroscopic pK_a s to experimental macroscopic pK_a s
237 when there could multiple numbers of each reported for each molecule? Experimental data in this case did not provide any
238 information that would indicate the titration site, the overall charge or the tautomer composition of macrostate pairs that are
239 associated with each measured macroscopic pK_a that can guide the matching.

240 For evaluating predictions taking the experimental data as reference Fraczkiewicz et al. delinited recommendations for fair
241 comparative analysis of computational pK_a predictions [14]. In the absence any experimental information that would aid the
242 match, experimental and computational pK_a s should be matched preserving the order of pK_a values and minimizing sum of
243 absolute errors.

244 We picked Hungarian matching algorithm [15, 16] to assign experimental and predicted macroscopic pK_a s with squared error
245 cost function as suggested by Kiril Lanevskij. The algorithm is available in SciPy package (`scipy.optimize.linear_sum_assignment`) [17].
246 This matching algorithm provides optimum global assignment that minimizes linear sum of squared errors of all pairwise
247 matches. The reason to select squared error cost function instead of absolute error cost function is to avoid misordered matches,
248 For instance, for a molecule with experimental pK_a values of 4 and 6, and predicted pK_a s of 7 and 8, Hungarian matching with
249 absolute error cost function would match 6 to 7 and 4 to 9. Hungarian matching with squared error cost would match 4 to 7
250 and 6 to 9, preserving the increasing pK_a value order between experimental and predicted values. A weakness of this approach
251 would be failing to match experimental value of 6 to predicted value of 7, if that was the correct match based on underlying
252 macrostates. But underlying pair of states were unknown to us both because experimental data of the challenge did not con-
253 tain information about what charge states the transitions were happening between and also because we have not collected the
254 pair of macrostates associated with each pK_a predictions in submissions. There is no perfect solution to numerical pK_a assign-
255 ment problem, but we tried to determine the most fair way to penalize predictions based on their numerical deviation from the
256 experimental values.

257 For the analysis of microscopic pK_a predictions we adopted a different matching approach. Only for the 8 molecules, we util-
258 ized the dominant microstate sequence inerfered from NMR experiments to match computational predictions and experimental
259 pK_a s. We will refer to this assignment method as microstate matching, where experimental pK_a value is matched to the com-
260 putational microscopic pK_a value which was reported for the dominant microstate pair observed for each transition. We have
261 compared the results of Hungarian matching and microstate matching.

262 Inevitably the choice of matching algorithms to assign experimental and predicted values has an impact on the calculation
263 of performance statistics. We believe the Hungarian algorithm for numerical matching and microstate-based were the best
264 choices, providing the most unbiased matching without introducing assumptions outside of the experimental data.

265 2.3.2 Statistical metrics for submission performance

266 A variety of accuracy and correlation statistics were considered for analyzing and comparing performance of predictions meth-
267 ods submitted to the SAMPL6 pK_a Challenge. Calculated performance statistics of predictions were provided to participants
268 before the workshop. Details of the analysis and scripts are maintained on the SAMPL6 Github Repository (described in Section
269 5).

270 There are six error metrics reported for the numerical error of the pK_a values: the root-mean-squared error (RMSE), mean ab-
271 solute error (MAE), mean error (ME), coefficient of determination (R^2), linear regression slope (m), and Kendall's Rank Correlation
272 Coefficient (τ). Uncertainty in each performance statistic was calculated as 95% confidence intervals estimated by bootstrapping
273 over predictions with 10000 bootstrap samples. Calculated errors statistics of all methods can be found in Table S2 for macro-
274 scopic pK_a predictions and Tables S4 and S4 for microscopic pK_a predictions.

275 In addition to the numerical error aspect of the pK_a values, we have also evaluated predictions in terms of their ability to cap-
276 ture the correct macrostates (ionization states) and microstates (tautomers of each ionization state) to the extend possible from
277 the available experimental data. For macroscopic pK_a s experiments did not provide any evidence of the identity of the ionization
278 states. However, the number of ionization states indicates the number of macroscopic pK_a s that exists between experimental
279 range of 2.0-12.0. For instance, SM14 has two experimental pK_a s and therefore 3 different charge states were observed between

the pH range of 2.0-12.0. If a prediction reported 4 macroscopic pK_a s, it is clear that this method predicted an extra ionization state. With this perspective we reported the number of unmatched experimental pK_a s (the number of missing pK_a predictions, i.e. missing ionization states) and the number of unmatched predicted pK_a s (the number of extra pK_a predictions, i.e. extra ionization states) after Hungarian matching. The later count was restricted to only predictions with pK_a values between 2 and 12, because that was the range of the experimental method. Errors in extra or missing pK_a prediction errors highlight failure to predict the correct number of ionization states within a pH range.

For the evaluation of microscopic pK_a predictions, taking advantage of the available dominant microstate sequence data for a subset of 8 compounds, we calculated the dominant microstate prediction accuracy. Dominant microstate prediction accuracy is the ratio of correct dominant tautomer predictions for each charge state divided by, calculated over all ionization states of each molecule. In order to extract the sequence of dominant microstates from the microscopic pK_a predictions sets, we calculated the relative free energy of microstates selecting a neutral tautomer and pH 0 as reference following the Equation 8. Calculation of relative free energy of microstates was explained in more detail in a previous publication [18].

Relative free energy of state with respect to reference state B at pH 0.0 (arbitrary pH value selected as reference) can be calculated as follows:

$$\Delta G_{AB} = \Delta m_{AB} RT \ln 10 (pH - pK_a) \quad (8)$$

Δm_{AB} is equal to the number protons in state A minus state B. R and T indicate molar gas constant and temperature, respectively. By calculating relative free energies of all predicted microstates with respect to the same reference state and pH, we were able to determine the sequence of predicted dominant microstates. The dominant tautomer of each charge state was determined as the the microstate with the lowest free energy in the subset of predicted microstates of each ionization state. This approach is feasible because the relative free energy of tautomers of the same ionization state is independent of pH and therefore the choice of reference pH is arbitrary.

We created a shortlist of top-performing methods for macroscopic and microscopic pK_a predictions. Top macroscopic pK_a predictions were selected based on the following criteria of consistence performance among different metrics: ranking in the top 10 consistently according to two error (RMSE, MAE) and two correlation metrics (R-Squared, and Kendall's Tau), and also havin a combined count of less than 8 missing or extra macroscopic pK_a s for the entire molecule set (a third of the number of compounds). These methods are presented in Table 2. A separate list of top performing methods were selected for microscopic pK_a with the following criteria: ranking in the top 10 methods when ranked by accuracy statistics (RMSE and MAE) and perfect dominant microstate prediction accuracy. These methods are presented in Table 3.

In addition to comparing the performance comparison of methods, we also wanted to compare pK_a prediction performance on the level of molecules to determine pK_a s of which molecules in the challenge set were harder to predict considering all the methods in the challenge. For this purpose, we plotted prediction error distributions of each molecule considering all prediction methods. We also calculated MAE for each molecule's over all predictions as well as for predictions from each method category.

2.4 Reference calculations

Including null model as helpful in comparative performance analysis of predictive methods to establish what the performance statistics look like for a baseline method for the specific dataset. Null models or null predictions employ a simple prediction model which is not expected to be particularly successful, but it is useful for providing a simple point of comparison for more sophisticated methods. The expectation is for more sophisticated or costly prediction methods to outperform the predictions from a null model, otherwise the simpler null model would be preferable. In SAMPL6 pK_a Challenge there were two blind submissions that database lookup methods that were suitable to be considered as null predictions. These methods, with submission IDs 5nm4j and 5nm4j both used OpenEye pKa-Prospector database to find the most similar molecule to query molecule and report its pK_a as predicted value. We acknowledge that database lookup methods with a rich experimental database presents a challenging null model to beat, however, due to the accuracy level needed from pK_a predictions for computer-aided drug design we believe it is an appropriate performance baseline that physical and empirical pK_a prediction methods should strive to perform better than.

We have also included additional reference calculations in the comparative analysis to provide more perspective. The methods we chose to include as reference calculations were missing from the blind predictions sets although they are widely used methods by academia and industry. representing different methodological approaches: Schrodinger/Epik (nb007, nb008, nb010), Schrodinger/Jaguar (nb011, nb013), Chemaxon/Chemicalize (nb015), and Molecular Discovery/MoKa (nb016, nb017). Epik and

327 Jaguar p_K_a predictions were collected by Bas Rustenburg, Chemicalize predictions by Mehtap Isik, and MoKa predictions by
328 Thomas Fox, after the challenge deadline avoiding any alterations to the respective standard procedures of the methods and
329 guidance of the experimental date. Reference calculations were not formally blind, as experimental data of the challenge has
330 been made publically available before their collection.

331 All figures and statistics tables in this manuscript include reference calculations. As the reference calculations were not formal
332 submissions, these were omitted from formal ranking in the challenge, but we present plots in this article which show them for
333 easy comparison. These are labeled with submission IDs of the form *nb###* to allow easy recognition of non-blind reference
334 calculations.

335 3 Results and Discussion

336 Participation to SAMPL6 p_K_a Challenge was high with 11 research groups contributing p_K_a prediction sets of 37 methods. A large
337 variety of p_K_a prediction methods were represented in SAMPL6 Challenge. We categorized these submissions into four method
338 categories: database lookup (DL), linear free energy relationship (LFER), quantitative structure property relationship or machine
339 learning (QSPR/ML), and quantum mechanics (QM). Quantum mechanics models were subcategorized into QM methods with
340 and without linear empirical correction (LEC), and combined quantum mechanics and molecular mechanics (QM + MM). Table 1
341 presents, method names, submission IDs, method categories, and also references of each approach. Integral equation-based
342 approaches (e.g. EC-RISM) were also evaluated under the Physical (QM) category. There were 2 DL, 4 LFER, and 5 QSPR/ML
343 methods represented in the challenge, including the reference calculations. Majority of QM calculations include linear empirical
344 corrections (22 methods in QM + LEC category), and only 5 QM methods were submitted without any empirical corrections.
345 There were 4 methods that used a mixed physical modeling approach of QM + MM.

346 The following sections present detailed performance evaluation of blind submissions and reference prediction methods for
347 macroscopic and microscopic p_K_a predictions. Performance statistics of all the methods can be found in Tables S2 and S4.
348 Methods are referred to by their submission ID's which are provided in Table 1.

349 3.1 Analysis of macroscopic p_K_a predictions

350 The performance of macroscopic p_K_a predictions were analyzed by comparison to experimental p_K_a values collected by the
351 spectrophotometric method via numerical matching following the Hungarian method. Overall p_K_a prediction performance was
352 lower than we have hoped for. Fig. 2 shows RMSE calculated for each prediction method represented by their submission IDs.
353 Other performance statistics are depicted in Fig. 3. In both figures method categories were indicated by the color of the error
354 bars. Statistics depicted in these figures can be found in Table S2. Prediction error ranged between 0.7 to 3.2 p_K_a units in terms
355 of RMSE, while an RMSE between 2-3 log units was observed for the majority of methods (20 out of 38 methods). Only five meth-
356 ods achieved RMSE less than 1 p_K_a unit. One is QM method with COSMO-RS approach for solvation and linear empirical cor-
357 rection (*xvxzd* (DSD-BLYP-D3(BJ)/def2-TZVPD//PBEh-3c[DCOSMO-RS] + RRHO(GFN-xTB[GBSA]) + Gsolv(COSMO-RS[TZVPD]) and
358 linear fit)), and the remaining four are empirical prediction methods of LFER (*xmyhm* (ACD/pKa Classsic), *nb007* (Schrodinger/Epk
359 Scan)) and QSPR/ML categories (*gyuhx* (Simulations Plus), *nb017* (MoKa)). These five methods with RMSE less than 1 p_K_a unit also
360 are the methods that have the lowest MAE. *xvxzd* and *xmyhm* were the only two methods for which the upper 95% confidence
361 interval of RMSE was lower than 1 p_K_a unit.

362 In terms of correlation statistics performance of many methods have good performance, although the ranking of methods
363 change R² and Kendall's Tau and many methods are indistinguishable from one another considering uncertainty of the correla-
364 tion statistics. 32 out of 38 methods have R higher than and Kendall's Tau higher than 0.7 and 0.6, respectively. 8 methods have
365 R² higher than 0.9 and 6 methods have Kendall's Tau higher than 0.8. The overlap of these two sets are the following: *gyuhx* (Sim-
366 ulations Plus), *xvxzd* (DSD-BLYP-D3(BJ)/def2-TZVPD//PBEh-3c[DCOSMO-RS] + RRHO(GFN-xTB[GBSA]) + Gsolv(COSMO-RS[TZVPD])
367 and linear fit), *xmyhm* (ACD/pKa Classic), *ryzue* (Adiabatic scheme with single point correction: MD/M06-2X//6-311++G(d,p)//M06-
368 2X/6-31+G(d) for bases and SMD/M06-2X//6-311++G(d,p)//M06-2X/6-31G(d) for acids + thermal corrections), and *5byn6* (Adiabatic
369 scheme: thermodynamic cycle that uses gas phase optimized structures for gas phase free energy and solution phase geo-
370 metries for solvent phase free energy. SMD/M06-2X/6-31+G(d) for bases and SMD/M06-2X/6-31G(d) for acids + thermal corrections).
371 It is worth noting that the *ryzue* and *5byn6* are QM predictions without any empirical correction. Their high correlation and rank
372 correlation coefficient scores signal that with an empirical correction their accuracy based performance could improve. Indeed,
373 the participants have showed that this is the case in their individual challenge analysis paper and achieved RMSE of 0.73 p_K_a
374 units after the challenge [27].

Table 1. Submission IDs, names, category, and type for all the pKa prediction sets. Reference calculations are labeled as nb###. The method name column lists the names provided by each participant in the submission file. The “type” column indicates if submission was or a post-deadline reference calculation, denoted by “Blind” or “Reference” respectively. The methods in the table are grouped by method category and not ordered by performance.

Method Category	Method	Microscopic pKa (Type I) Submission ID	Macroscopic pKa (Type III) Submission ID	Submission Type	Ref.
DL	Substructure matches to experimental data in pKa OpenEye pKa Prospector Database v1.0	<i>5nm4j</i>	Null	[19]	
DL	OpenEye pKa-Prospector 1.0.0.3 with Analog Search ion identification algorithm	<i>pwn3m</i>	Null	[19]	
LFER	ACD/pKa GALAS (ACD/Percepta Kernel v1.6)	<i>v8qph</i>	<i>37xm8</i>	Blind	[20]
LFER	ACD/pKa Classic (ACD/Percepta Kernel, v1.6)		<i>xmyhm</i>	Blind	[21]
LFER	Epik Scan (Schrodinger v2017-4)		<i>nb007</i>	Reference	[22]
LFER	Epik Microscopic (Schrodinger v2017-4)	<i>nb008</i>	<i>nb010</i>	Reference	[22]
QSPR/ML	OpenEye Gaussian Process	<i>6tvf8</i>	<i>hytjn</i>	Blind	[10]
QSPR/ML	OpenEye Gaussian Process Resampled		<i>q3pfj</i>	Blind	[10]
QSPR/ML	S+pKa (ADMET Predictor v8.5, Simulations Plus)	<i>hdijq</i>	<i>gyuhx</i>	Blind	[23]
QSPR/ML	Chemicalize v18.23 (ChemAxon MarvinSketch v18.23)		<i>nb015</i>	Reference	[24]
QSPR/ML	Moka v3.1.3	<i>nb016</i>	<i>nb017</i>	Reference	[25, 26]
QM	Adiabatic scheme with single point correction: SMD/M06-2X//6-311++G(d,p)//M06-2X//6-31+G(d) for bases and SMD/M06-2X//6-311++G(d,p)//M06-2X//6-31G(d) for acids + thermal corrections	<i>ko8yx</i>	<i>ryzue</i>	Blind	[27]
QM	Direct scheme with single point correction: SMD/M06-2X//6-311++G(d,p)//M06-2X//6-31G(d) for bases and SMD/M06-2X//6-311++G(d,p)//M06-2X//6-31G(d) for acids + thermal corrections	<i>w4z0e</i>	<i>xikp8</i>	Blind	[27]
QM	Adiabatic scheme: thermodynamic cycle that uses gas phase optimized structures for gas phase free energy and solution phase geometries for solvent phase free energy. SMD/M06-2X//6-31+G(d) for bases and SMD/M06-2X//6-31G(d) for acids + thermal corrections	<i>wcvnu</i>	<i>5byn6</i>	Blind	[27]
QM	Vertical scheme: thermodynamic cycle that uses only gas phase optimized structures to compute gas phase and solvation free energy. SMD/M06-2X//6-31+G(d) for bases and SMD/M06-2X//6-31G(d) for acids + Thermal corrections	<i>arcko</i>	<i>w4iyd</i>	Blind	[27]
QM	Direct scheme: solution phase free energy is determined by solution phase geometries without thermodynamic cycle SMD/M06-2X//6-31+G(d) for bases and SMD/M06-2X//6-31G(d) for acids + thermal corrections	<i>wexjs</i>	<i>y75vj</i>	Blind	[27]
QM + LEC	Jaguar (Schrodinger v2017-4)	<i>nb011</i>	<i>nb013</i>	Reference	[28]
QM + LEC	CPCM/B3LYP/6-311+G(d,p) and global fitting	<i>y4wws</i>	<i>35bdm</i>	Blind	[8]
QM + LEC	CPCM/B3LYP/6-311+G(d,p) and separate fitting for neutral to negative and for positive to neutral transformations	<i>qsicn</i>	<i>p0jba</i>	Blind	[8]
QM + LEC	EC-RISM/MP2/6-311+G(d,p)-P3NI-q-noThiols-2par	<i>kxzt</i>	<i>ds62k</i>	Blind	[29]
QM + LEC	EC-RISM/MP2/cc-pVTZ-P2-q-noThiols-2par	<i>ftc8w</i>	<i>2ii2g</i>	Blind	[29]
QM + LEC	EC-RISM/MP2/6-311+G(d,p)-P2-phi-all-2par	<i>ktpj5</i>	<i>nb001</i>	Blind*	[29]
QM + LEC	EC-RISM/MP2/6-311+G(d,p)-P2-phi-noThiols-2par	<i>wuuvc</i>	<i>nb002</i>	Blind*	[29]
QM + LEC	EC-RISM/MP2/6-311+G(d,p)-P3NI-phi-all-2par	<i>2umai</i>	<i>nb003</i>	Blind*	[29]
QM + LEC	EC-RISM/MP2/6-311+G(d,p)-P3NI-phi-noThiols-2par	<i>cm2yq</i>	<i>nb004</i>	Blind*	[29]
QM + LEC	EC-RISM/MP2/6-311+G(d,p)-P2-phi-all-1par	<i>z7fhp</i>	<i>nb005</i>	Blind*	[29]
QM + LEC	EC-RISM/MP2/6-311+G(d,p)-P3NI-phi-all-1par	<i>8toyp</i>	<i>nb006</i>	Blind*	[29]
QM + LEC	EC-RISM/MP2/cc-pVTZ-P2-phi-noThiols-2par	<i>epvmk</i>	<i>tjtd0</i>	Blind	[29]
QM + LEC	EC-RISM/MP2/cc-pVTZ-P2-phi-all-2par	<i>xnoe0</i>	<i>mkhqa</i>	Blind	[29]
QM + LEC	EC-RISM/MP2/cc-pVTZ-P3NI-phi-noThiols-2par	<i>4o0ia</i>	<i>mpwiy</i>	Blind	[29]
QM + LEC	EC-RISM/B3LYP/6-311+G(d,p)-P3NI-q-noThiols-2par	<i>nxaaw</i>	<i>ad5pu</i>	Blind	[29]
QM + LEC	EC-RISM/B3LYP/6-311+G(d,p)-P3NI-phi-noThiols-2par	<i>0xi4b</i>	<i>f0gew</i>	Blind	[29]
QM + LEC	EC-RISM/B3LYP/6-311+G(d,p)-P2-phi-noThiols-2par	<i>cwyk</i>	<i>np6b4</i>	Blind	[29]
QM + LEC	PCM/B3LYP/6-311+G(d,p)	<i>gdqeg</i>	<i>yc70m</i>	Blind	[29]
QM + LEC	COSMOtherm_FINE17 (COSMOtherm C30_1701, BP/TZVPD/FINE//BP/TZVP/COSMO)	<i>t8ewk</i>	<i>0hxtm</i>	Blind	[30, 31]
QM + LEC	DSD-BLYP-D3(BJ)/def2-TZVPD//PBEh-3c[DCOSMO-RS] + RRHO[GFN-xTB[GBSA]] + Gsolv(COSMO-RS[TZVPD]) and linear fit		<i>xvxzd</i>	Blind	[32]
QM + LEC	ReScosS conformations // DSD-BLYP-D3 reranking // COSMOtherm pKa: DSD-BLYP-D3(BJ)/def2-TZVPD// PBE-D3(BJ)/def2-TZVP/COSMO + RRHO[GFN-xTB + GBSA-water] + Gsolv[COSMO-RS(FINE17/TZVPD)] level and COSMOtherm pKa applied at the single conformer pair level (COSMOtherm17.0.5 release and BP-TZVPD-FINE-C30-1701 parameterization)	<i>eyetm</i>	<i>8xt50</i>	Blind	[32]
QM + LEC	ReScosS conformations // COSMOtherm pKa: DSD-BLYP-D3(BJ)/def2-TZVPD// PBE-D3(BJ)/def2-TZVP/COSMO + RRHO[GFN-xTB + GBSA-water] + Gsolv[COSMO-RS(FINE17/TZVPD)] level and COSMOtherm pKa was applied directly on the resulting conformer sets with at least 5% Boltzmann weights for each microspecies (COSMOtherm17.0.5 release and BP-TZVPD-FINE-C30-1701 parameterization)	<i>ccpmw</i>	<i>yqkga</i>	Blind	[32]
QM + MM	M06-2X//6-31G*(for bases) or 6-31+G*(for acids) for gas phase, solvation free energy using TI with explicit solvent and GAFF, solvation free energy of proton -265.6 kcal/mol	<i>0wfzo</i>		Blind	[33]
QM + MM	M06-2X//6-31G*(for bases) or 6-31+G*(for acids) for gas phase, solvation free energy using TI with explicit solvent and GAFF, solvation free energy of proton -271.88 kcal/mol	<i>z3btx</i>		Blind	
QM + MM	M06-2X//6-31G*(for bases) or 6-31+G*(for acids) + thermal state correction for gas phase, solvation free energy using TI with explicit solvent and GAFF, solvation free energy of proton -265.6 kcal/mol	<i>758j8</i>		Blind	
QM + MM	M06-2X//6-31G*(for bases) or 6-31+G*(for acids) + thermal state correction for gas phase, solvation free energy using TI with explicit solvent and GAFF, solvation free energy of proton -271.88 kcal/mol	<i>hgn83</i>		Blind	

* Microscopic pKa submissions were blind, however, participant requested a correction after blind submission deadline for macroscopic pKa submissions. Therefore, these were assigned submission IDs in the form of nb##.

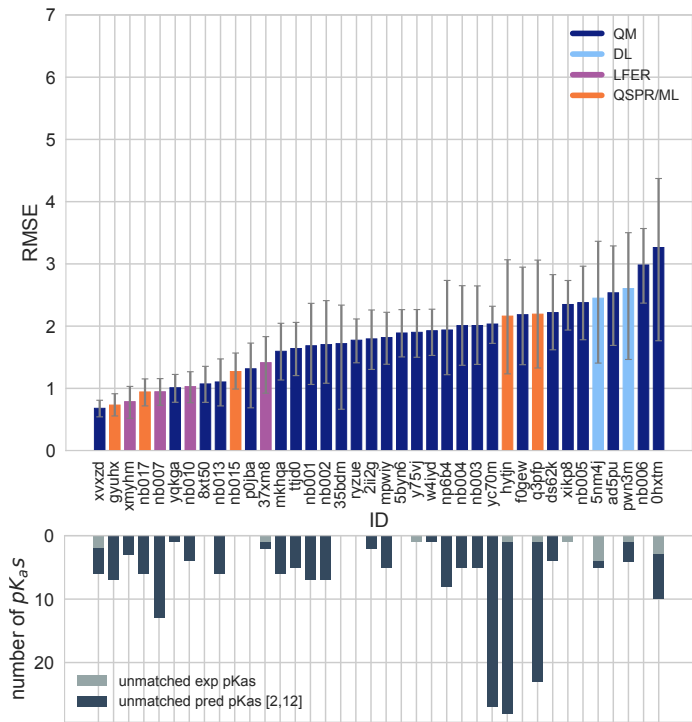


Figure 2. RMSE and unmatched pK_a counts vs. submission ID plots for macroscopic pK_a predictions based on Hungarian matching. Methods are indicated by submission IDs. RMSE is shown with error bars denoting 95% confidence intervals obtained by bootstrapping over challenge molecules. Submissions are colored by their method categories. Light blue colored database look up methods are utilized as the null prediction method. QM methods (navy) includes pure QM, QM+LEC, and QM+MM approaches. Lower bar plots show the number of unmatched experimental pK_a s (light grey, missing predictions) and the number of unmatched pK_a predictions (dark grey, extra predictions) for each method between pH 2 and 12. Submission IDs are summarized in Table 1. Submission IDs of the form *nb###* refer to non-blinded reference methods computed after the blind challenge submission deadline. All others refer to blind, prospective predictions.

Null prediction methods based on database lookup (*5nm4j* and *pwn3m*) had similar performance, roughly RMSE of 2.5 pK_a units, MAE of 1.5 pK_a units, R^2 of 0.2 and Kendall's Tau of 0.3. Many methods were observed to have prediction performance advantage over the Null predictions shown in light blue in Fig. 2 and Fig. 3 considering all the performance metrics as a whole. In terms of correlation statistics the null methods are the worst performers, except *0hxtm*. From the perspective of accuracy-based statistics (RMSE and MAE), only the top 10 methods were observed to have significantly lower errors than the null methods considering the uncertainty of error metrics expressed as 95% confidence intervals.

Distribution of macroscopic pK_a prediction signed errors observed in each submission was plotted in Fig. 7A as ridge plots based on Hungarian matching. *2ii2g*, *f0gew*, *np64b*, *p0jba*, and *yc70m* tend to overestimate and *5byn6*, *ryzue*, and *w4yjd* tend to underestimate macroscopic pK_a values.

There were four submissions of QM+LEC category that used COSMO-RS implicit solvation model. It was interesting that while three of these achieved the lowest RMSE among QM-based methods (*xvxzd*, *yqkga*, and *8xt50*) [32] and one of them showed the highest RMSE (*0hxtm* (COSMOtherm_FINE17)) in SAMPL6 Challenge macroscopic pK_a predictions. All four methods used COSMO-RS/FINE17 level to compute solvation free energies. The major difference between the three low-RMSE methods and the *0hxtm* seems to be the protocol for determining relevant conformations for each microstate. *xvxzd*, *yqkga*, and *8xt50* methods used semi-empirical tight binding (GFN-xTB) method and GBSA continuum solvation model for geometry optimization of conformers and followed up with high level single point energy calculations with solvation free energy (COSMO-RS(FINE17/TZVPD)) and rigid rotor harmonic oscillator (RRHO[GFN-xTB(GBSA)] corrections. *yqkga*, and *8xt50* methods selected conformations for each microstate with Relevant Solution Conformer Sampling and Selection (ReSCoSS) workflow. Conformations were clustered according to shape and lowest energy conformations from each cluster according to BP86/TZVP/COSMO single point energies in any of the 10 different COSMO-RS solvents were considered as relevant conformers. More details of the ReSCoSS workflow was described by Pracht et al [32] *yqkga* method further filtered out conformers that have less than 5% Boltzmann weights at the DSD-

396 BLYP-D3/def2-TZVPD + RRHO(GFNxTB) + COSMO-RS(fine) level. *xvxzd* method used MF-MD-GC//GFN-xTB workflow and used
397 energy thresholds of 6 kcal/mol and 10 kcal/mol, for conformer and microstate selection On the other hand, the conformational
398 ensemble captured for each microstate seems to be much limited for *0hxtm* method, judging by the method description in the
399 submission file. *0hxtm* method reported that relevant conformations were computed with the COSMOconf 4.2 workflow which
400 produced multiple relevant conformers for only the neutral states of SM18 and SM22. In contrast to *xvxzd*, *yqkga*, and *8xt50*
401 methods, the *0hxtm* method also did not include a RRHO correction. Participants of the three low-RMSE methods report that
402 capturing the chemical ensemble for each molecule including conformers and tautomers and high level QM calculations led to
403 more successful macroscopic pK_a prediction results and RRHO correction provided a minor improvement [32]. Comparing these
404 results to other QM approaches in SAMPL Challenge also points to the advantage of COSMO-RS solvation approach compared
405 to other implicit solvent models.

406 In addition the statistics related to the value of pK_a , we have also analyzed missing or extra pK_a predictions. Analysis of the
407 pK_a values with accuracy- and correlation-based error metrics was only possible after assignment of predicted macroscopic pK_a s
408 to experimental pK_a s through the Hungarian matching, although, this approach masks pK_a prediction issues in the form of extra
409 or missing macroscopic pK_a predictions. To capture this form of prediction errors we reported the number of unmatched ex-
410 perimental pK_a s (missing pK_a predictions and the number of unmatched predicted pK_a s (extra pK_a predictions) after Hungarian
411 matching for each method. Both missing and extra pK_a prediction counts were only considered for the pH range of 2-12 which
412 was the limits of experimental measurements. The lower subplot of Fig. 2 shows the total count of unmatched experimental or
413 predicted pK_a s for all the molecules in each prediction set. The order of submission IDs in the x-axis follows the RMSD based
414 ranking so that the performance of each methods from both pK_a value accuracy and the number of pK_a s can be viewed together.
415 Presence of missing or extra macroscopic pK_a predictions is a critical error, because inaccuracy in predicting the correct num-
416 ber of macroscopic transitions shows that methods are failing predict the correct set of charge states, i.e. failing to predict the
417 correct number of ionization states that can be observed between the specified pH range.

418 In challenge results, extra macroscopic pK_a predictions were found to be more common than missing pK_a predictions. In
419 pK_a prediction evaluations usually accuracy of ionization states predicted within a pH range seen is neglected. When predictions
420 are only evaluated for pK_a value accuracy with numerical matching algorithms more pK_a predictions are likely to lead to lower
421 prediction errors. Therefore, it is not surprising that methods are biased to predict extra pK_a values. The SAMPL6 pK_a Challenge
422 experimental data consists of 31 macroscopic pK_a s in total, measured for 24 molecules (6 molecules in the set have multiple
423 pK_a s). Within the 10 methods with lowest RMSE only *xvxzd* method has an error of missing predicted pK_a (2 unmatched out
424 of 31 experimental pK_a s), and all other methods that rank top 10 according to RMSE have extra predicted pK_a s ranging from 1
425 to 13. Two prediction sets without any extra pK_a predictions and low RMSE are *8xt50* (ReSCoSS conformations // DSD-BLYP-D3
426 reranking // COSMOtherm pKa) and *nb015* (ChemAxon/Chemicalize).

427 3.1.1 Consistently well performing methods for macroscopic pK_a prediction

428 Methods ranked differently when ordered by different error metrics, although there were a couple of methods that consistently
429 ranked at the top fraction. By using a combinatorial criteria that takes all multiple statistical metrics and unmatched pK_a counts
430 into account, we identified a short list of consistently well performing methods for macroscopic pK_a predictions, shown in Table 2.
431 The criteria for selection was ranking in Top 10 according to RMSE, MAE, R^2 , and Kendall's Tau and also having a combined
432 unmatched pK_a (extra and missing pK_a s) count less than 8 (a third of the number of compounds). The resulted in a list of four
433 methods which are consistently well performing across all criteria.

434 Consistently well performing methods for macroscopic pK_a prediction included methods from all categories. Two methods of
435 the QM+LEC category were *xvxzd* (DSD-BLYP-D3(BJ)/def2-TZVPD//PBEh-3c[DCOSMO-RS] + RRHO(GFN-xTB[GBSA]) + Gsolv(COSMO-
436 RS[TZVPD])) and linear fit) and (*8xt50*) (ReSCoSS conformations // DSD-BLYP-D3 reranking // COSMOtherm pKa) and both used
437 COSMO-RS approach. Empirical pK_a predictions with top performance were both proprietary softwares. From QSPR and LFER
438 categories, *gyuhx* (Simulation Plus) and *xmyhm* (ACD/pKa Classic) were the methods that made it to consistently well perform-
439 ing methods list. Simulation Plus pK_a prediction method consisted of 10 artificial neural network ensembles trained on 16,000
440 compounds for 10 classes of ionizable atoms. Atom type and local molecular environment was how the ionization class of each
441 atom was determined [34]. ACD/pKa Classic which was trained on method 17,000 compounds uses Hammet-type equations
442 and tries to capture effects related to tautomeric equilibria, covalent hydration, resonance effects, and α , β -unsaturated systems
443 [21].

444 In Figure 4 prediction vs. experimental data correlation plots of macroscopic pK_a predictions with 4 consistently well-performing
445 methods, a representative average method, and the null method(*5nm4j*). The representative method with average performance

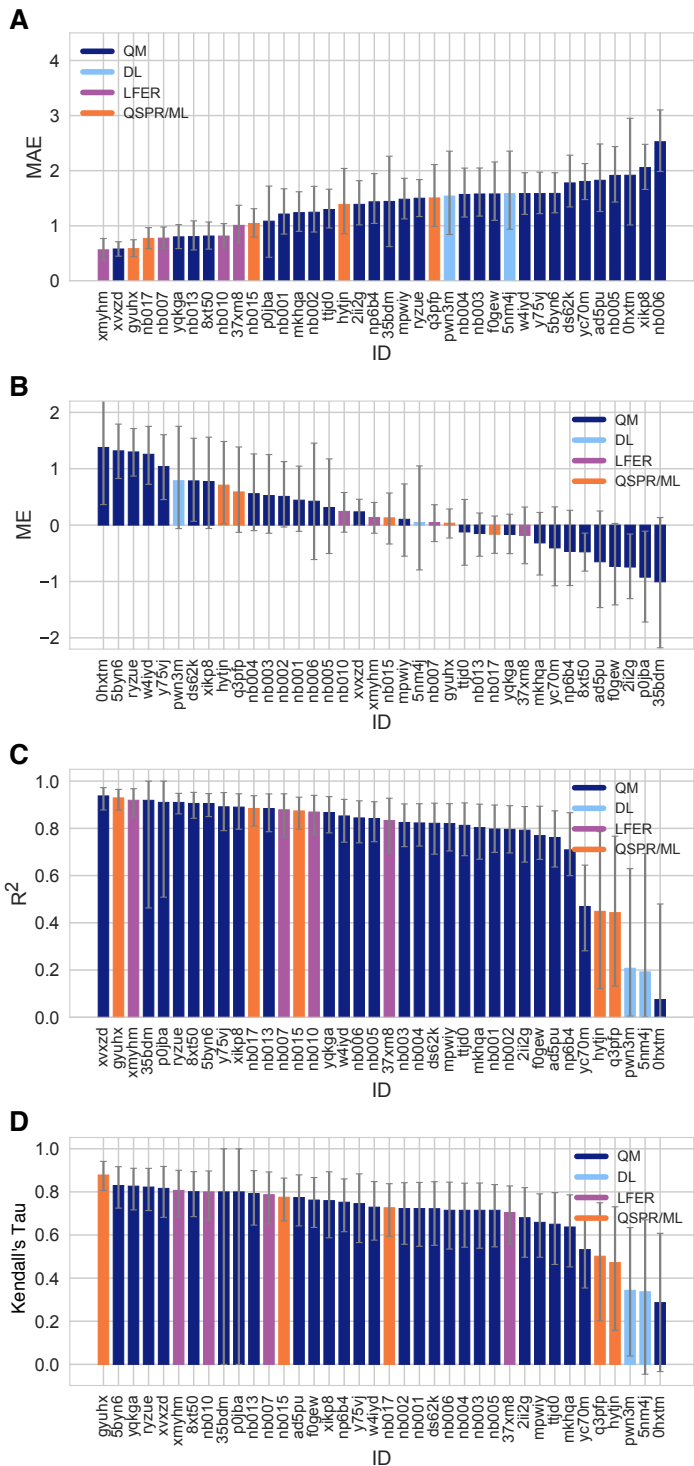


Figure 3. Additional performance statistics for macroscopic pK_a predictions based on Hungarian matching. Methods are indicated by submission IDs. Mean absolute error (MAE), mean error (ME), Pearson's R^2 , and Kendall's Rank Correlation Coefficient τ are shown, with error bars denoting 95% confidence intervals obtained by bootstrapping over challenge molecules. Refer to Table 1 for submission IDs and method names. Submissions are colored by their method categories. Light blue colored database look up methods are utilized as the null prediction method.

446 (2li2g (EC-RISM/MP2/cc-pVTZ-P2-q-noThiols-2par)) was selected as the method with the highest RMSE below the median of all
 447 methods.

Table 2. Four consistently well-performing prediction methods for macroscopic pK_a prediction based on consistent ranking within the Top 10 according to various statistical metrics. Submissions were ranked according to RMSE, MAE, R^2 , and τ . Consistently well-performing methods were selected as the ones that rank in the Top 10 in each of these statistical metrics. These methods also have less than 2 unmatched experimental pK_a s and less than 7 unmatched predicted pK_a s according to Hungarian matching. Performance statistics are provided as mean and 95% confidence intervals.

Submission ID	Method Name	RMSE	MAE	R^2	Kendall's Tau (τ)	Unmatched Exp. pK_a Count	Unmatched Pred. pK_a Count [2,12]
xvxzd	Full quantum chemical calculation of free energies and fit to experimental pK_a	0.68 [0.54, 0.81]	0.58 [0.45, 0.71]	0.94 [0.88, 0.97]	0.82 [0.68, 0.92]	2	4
gyuhx	S+pKa	0.73 [0.55, 0.91]	0.59 [0.44, 0.74]	0.93 [0.88, 0.96]	0.88 [0.8, 0.94]	0	7
xmyhm	ACD/pKa Classic	0.79 [0.52, 1.03]	0.56 [0.38, 0.77]	0.92 [0.85, 0.97]	0.81 [0.68, 0.9]	0	3
8xt50	ReSCoSS conformations // DSD-BLYP-D3 reranking // COSMOtherm pKa	1.07 [0.78, 1.36]	0.81 [0.58, 1.07]	0.91 [0.84, 0.95]	0.80 [0.68, 0.89]	0	0

448 3.1.2 Which chemical properties are driving macroscopic pK_a prediction failures?

449 In addition to comparing the performance of methods that participated in the SAMPL6 Challenge, we also wanted to analyze
 450 macroscopic pK_a predictions from the perspective of challenge molecules and determine whether particular compounds suffer
 451 from larger inaccuracy in pK_a predictions. The goal of this analysis is to provide guidance on which molecular properties or
 452 moieties might be causing larger pK_a prediction error. In Fig. 5 2D depictions of challenge molecules are presented with MAE cal-
 453 culated for their macroscopic pK_a predictions over all methods, based on Hungarian match. For multiprotic molecules MAE was
 454 averaged over all the pK_a s. For the analysis of pK_a prediction accuracy observed for each molecule, MAE is a more appropriate
 455 statistical value than RMSE for following global trends. This is because MAE value less sensitive to outliers than is RMSE.

456 A comparison of prediction performance of individual molecules is shown in Fig. 6. In Fig. 6A MAE each molecule is shown
 457 considering all blind predictions and reference calculations. A cluster of molecules marked orange and red have higher than
 458 average MAE. Molecules marked red (SM06, SM21, and SM22) are the only compounds in SAMPL6 dataset with bromo or iodo
 459 groups and they suffered a macroscopic pK_a prediction error in the range of 1.7-2.0 pK_a units in terms of MAE. Molecules marked
 460 orange (SM03, SM10, SM18, SM19, and SM20) all have sulfur-containing heterocycles, and all molecules except SM18 of this
 461 group have MAE larger than 1.6 pK_a unit. SM18 despite containing thiazole group has a low MAE. SM18 is the only compound
 462 with three experimental pK_a s and we suspect presence of multiple experimental pK_a s could have a masking effect on the errors
 463 captured by MAE with Hungarian matching due to more pairing choices.

464 We analyzing MAE of each molecule for empirical(LFER and QSPR/ML) and QM-based physical methods (QM, QM+LEC, and
 465 QM+MM) separately for more insight. Fig. 6B shows that the difficulty of predicting pK_a s of the same subset of molecules was
 466 a trend conserved in the performance of physical methods. For QM-based methods too sulfur containing heterocycles, amide
 467 next to aromatic heterocycles, compounds with iodo and bromo domains have lower pK_a prediction accuracy.

468 SAMPL6 pK_a set consists of only 24 small molecules which limits our ability to do statistically confirm the determination of
 469 which chemical substructures cause greater errors in pK_a predictions. Still the trends seen in this challenge distinguish molecules
 470 with iodo, bromo, and sulfur-containing heterocycles with larger prediction errors of macroscopic pK_a value. We hope that
 471 reporting this observation will lead to improvement of methods for similar compounds with such moieties.

472 We have also looked for correlation with molecular descriptors for finding other potential explanations for why macroscopic
 473 pK_a predictions were larger in some molecules. While testing correlation between errors and many molecular descriptors it
 474 is important to keep the possibility of spurious correlations in mind. We haven't observed any significant correlation between
 475 numerical pK_a predictions and the descriptors we have tested. First of all, higher number of experimental pK_a s (Fig. 6A) did not
 476 seem to associate with lower pK_a prediction performance. But we need to keep in mind that there was a low representation
 477 of multiprotic compounds in the SAMPL6 set (5 molecules with 2 macroscopic pK_a s and one molecule with 3 macroscopic pK_a s).
 478 Other descriptors we checked for were presence of amide groups, molecular weight, heavy atom count, rotatable bond count,
 479 heteroatom count, heteroatom to carbon ratio, ring system count, maximum ring size, and the number of microstates (as
 480 enumerated for the challenge). Correlation plots and R^2 values can be seen in Fig. S2. We had suspected that pK_a prediction
 481 methods may be trained better for moderate values (4-10) than extreme values as molecules with extreme pK_a s are less likely
 482 to change ionization states close to physiological pH. To test this we look at the distribution of absolute errors calculated for all
 483 molecules and challenge predictions binned by experimental pK_a value 2 pK_a unit increments. As can be seen in Fig. S3B, the
 484 value of true macroscopic pK_a s was not a factor affecting prediction error seen in SAMPL6 Challenge.

485 Fig. 7B is helpful to answer the question of "Are there molecules with consistently overestimated or underestimated pK_a s?".

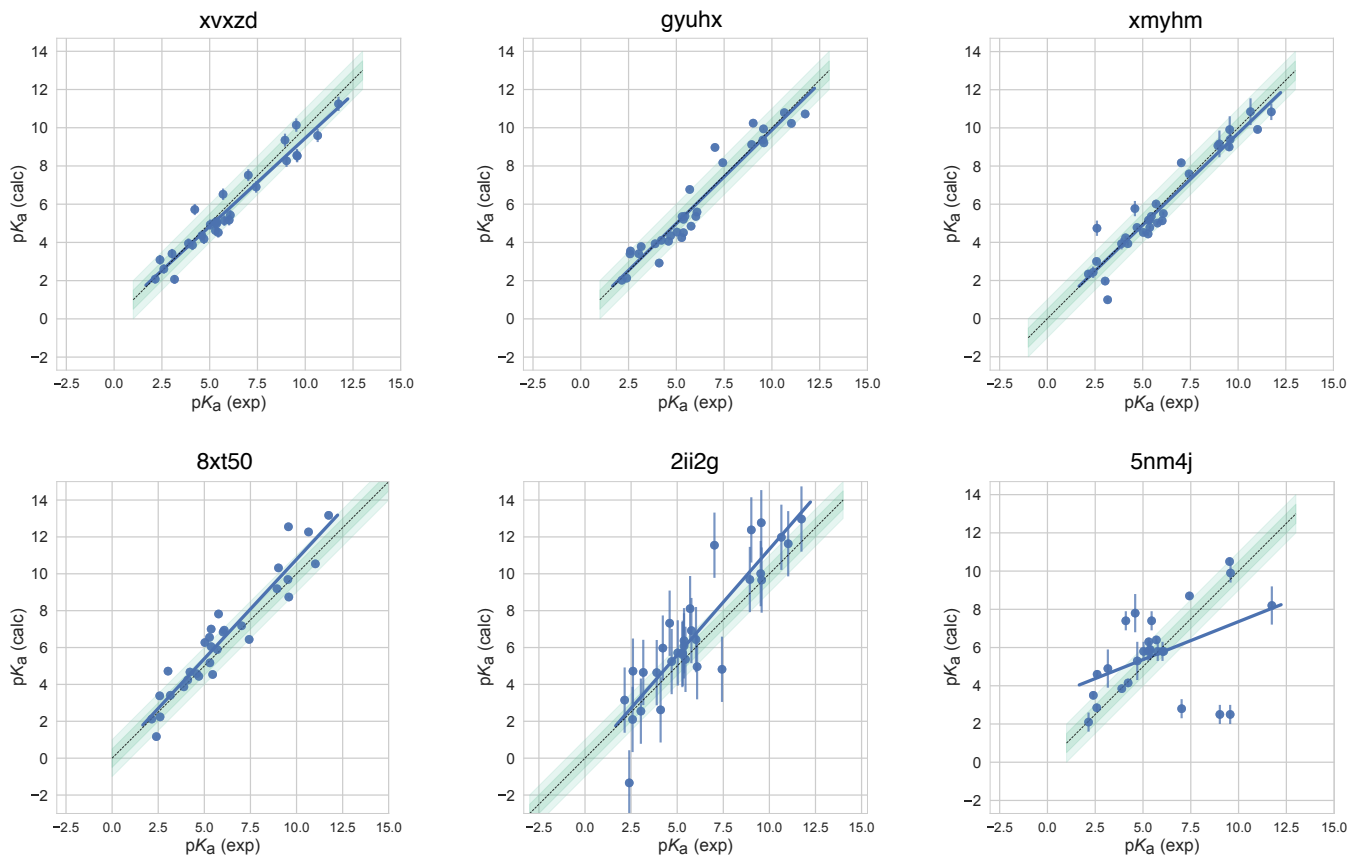


Figure 4. Predicted vs. experimental value correlation plots of 4 consistently well-performing methods, a representative method with average performance (2ii2g), and the null method (5nm4j). Dark and light green shaded areas indicate 0.5 and 1.0 units of error. Error bars indicate standard error of the mean of predicted and experimental values. Experimental pKa SEM values are too small to be seen under the data points. EC-RISM/MP2/cc-pVTZ-P2-q-noThiols-2par method (2ii2g) was selected as the representative method with average performance because it is the method with the highest RMSE below the median.

486 This ridge plots shows the error distribution of each experimental p K_a . SM02_pKa1, SM04_pKa1, SM14_pKa1, and SM21_pKa1
 487 were underestimated by majority of the prediction methods for more than 1 p K_a unit. SM03_pKa1, SM06_pKa2, SM19_pKa1, and
 488 SM20_pKa1 were overestimated by the majority of the preodction methods for more than 1 p K_a unit. SM03_pKa1, SM06_pKa2,
 489 SM10_pKa1, SM19_pKa1, and SM22_pKa1 have the highest spread of errors and were less accurately predicted overall. Refer to
 490 Ridge plots of Delta pKa error to identify compounds that were frequently mispredicted.

491 **3.2 Analysis of microscopic p K_a predictions using microstates determined by NMR for 8 molecules**
 492 The common approach for analysing microscopic p K_a prediction accuracy has been to compare it to experimental macroscopic
 493 p K_a data, assuming experimental p K_a s describe titrations of distinguishable sides and, therefore, equal to microscopic p K_a s. But
 494 this typical approach fails to evaluate the methods in microscopic level.

495 Analysis of microscopic p K_a predictions of the SAMPL6 Challenge was not straight-forward due to lack of experimental
 496 data with microscopic detail. For 24 molecules macroscopic p K_a s were determined with spectrophotometric method. For 18
 497 molecules single macroscopic titration was observed and for 6 molecules multiple experimental p K_a s were reported. For 18
 498 molecules with single experimental p K_a it is probabable that the molecules are monoprotic and therefore macroscopic p K_a
 499 value is equal to the microscopic p K_a , but there is no direct experimental evidence to support that this is the case but only
 500 the support from prediction methods. There is always the possibility that the macroscopic p K_a observed is the result of two
 501 different titrations overlapping closely with respect to pH. We did not want to bias the blind challenge analysis with any prediction
 502 method. Therefore, we believe analyzing the microscopic p K_a predictions via Hungarian matching to experimental values

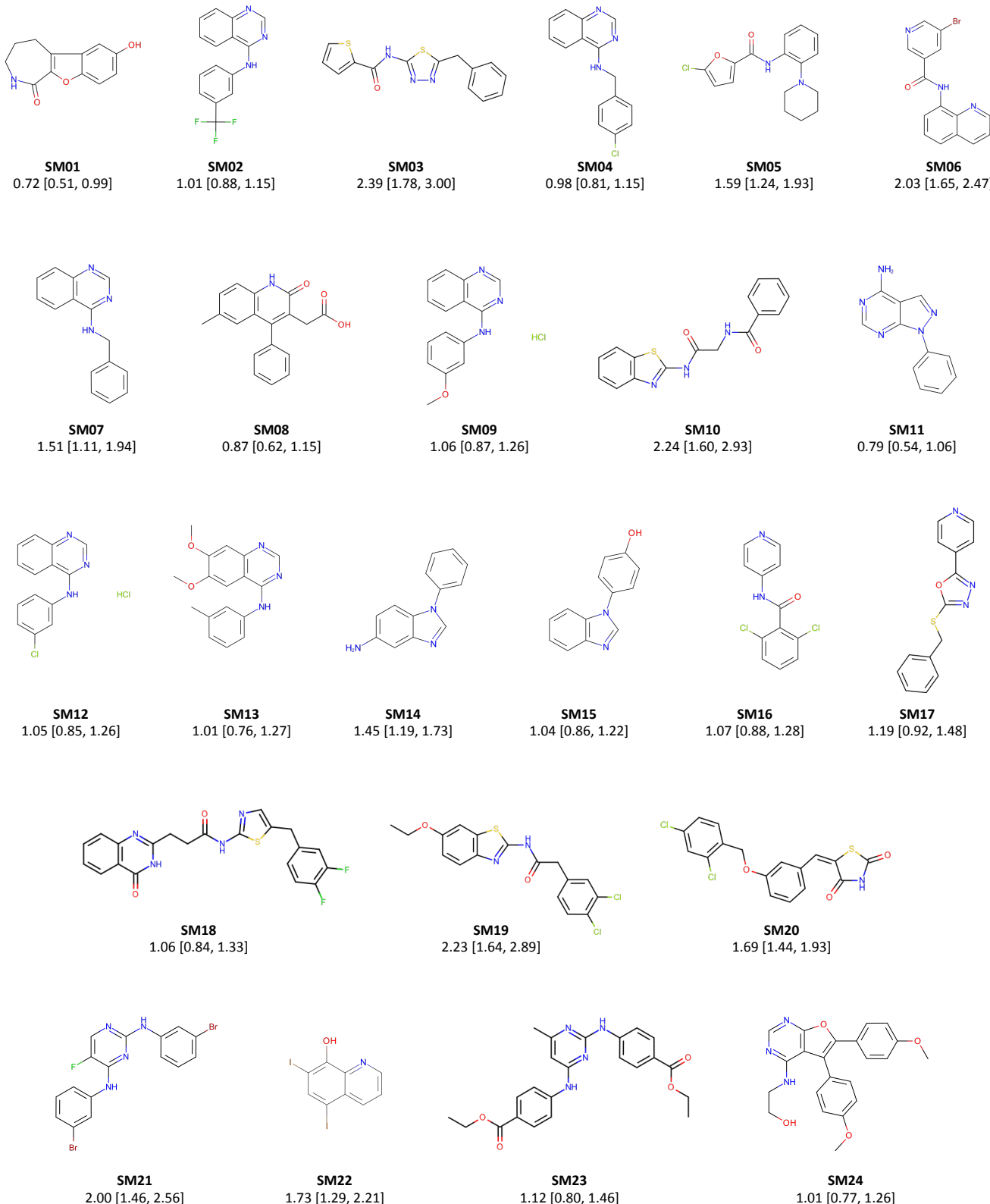
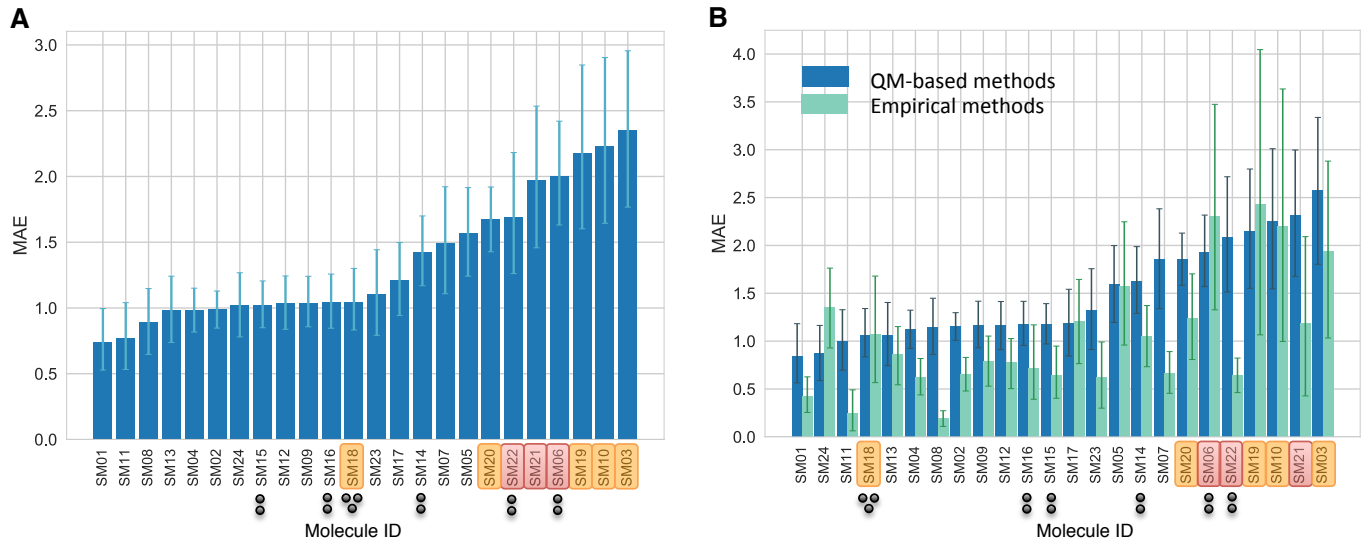
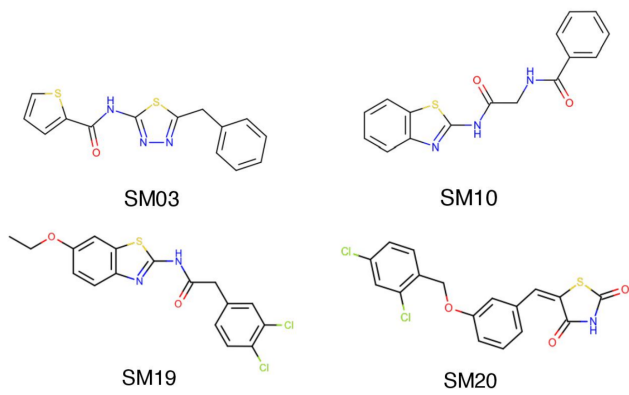


Figure 5. Molecules of SAMPL6 Challenge with MAE calculated for all macroscopic pK_a predictions. MAE calculated considering all prediction methods indicate which molecules had the lowest prediction accuracy in SAMPL6 Challenge. MAE values calculated for each molecule include all the matched pK_a values, which could be more than one per method for multiprotic molecules (SM06, SM14, SM15, SM16, SM18, SM22). Hungarian matching algorithm was employed for pairing experimental and predicted pK_a values. MAE values are reported with 95% confidence intervals.



C SAMPL6 molecules with sulfur-containing heterocycles



D SAMPL6 molecules with bromo and iodo groups

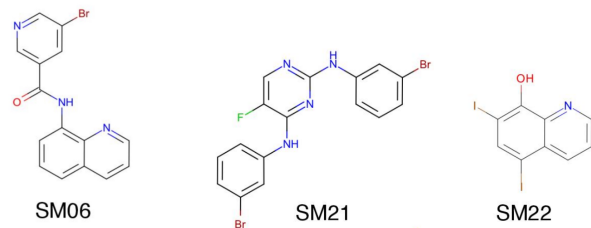


Figure 6. Average prediction accuracy calculated over all prediction methods was lower for molecules with sulfur-containing heterocycles, bromo, and iodo groups. (A) MAE calculated for each molecule as an average of all methods. (B) MAE of each molecule broken out by method category. QM-based methods (blue) include QM predictions with or without linear empirical correction. Empirical methods (green) include QSAR, ML, DL, and LFER approaches. (C) Depiction of SAMPL6 molecules with sulfur-containing heterocycles. (D) Depiction of SAMPL6 molecules with iodo and bromo groups.

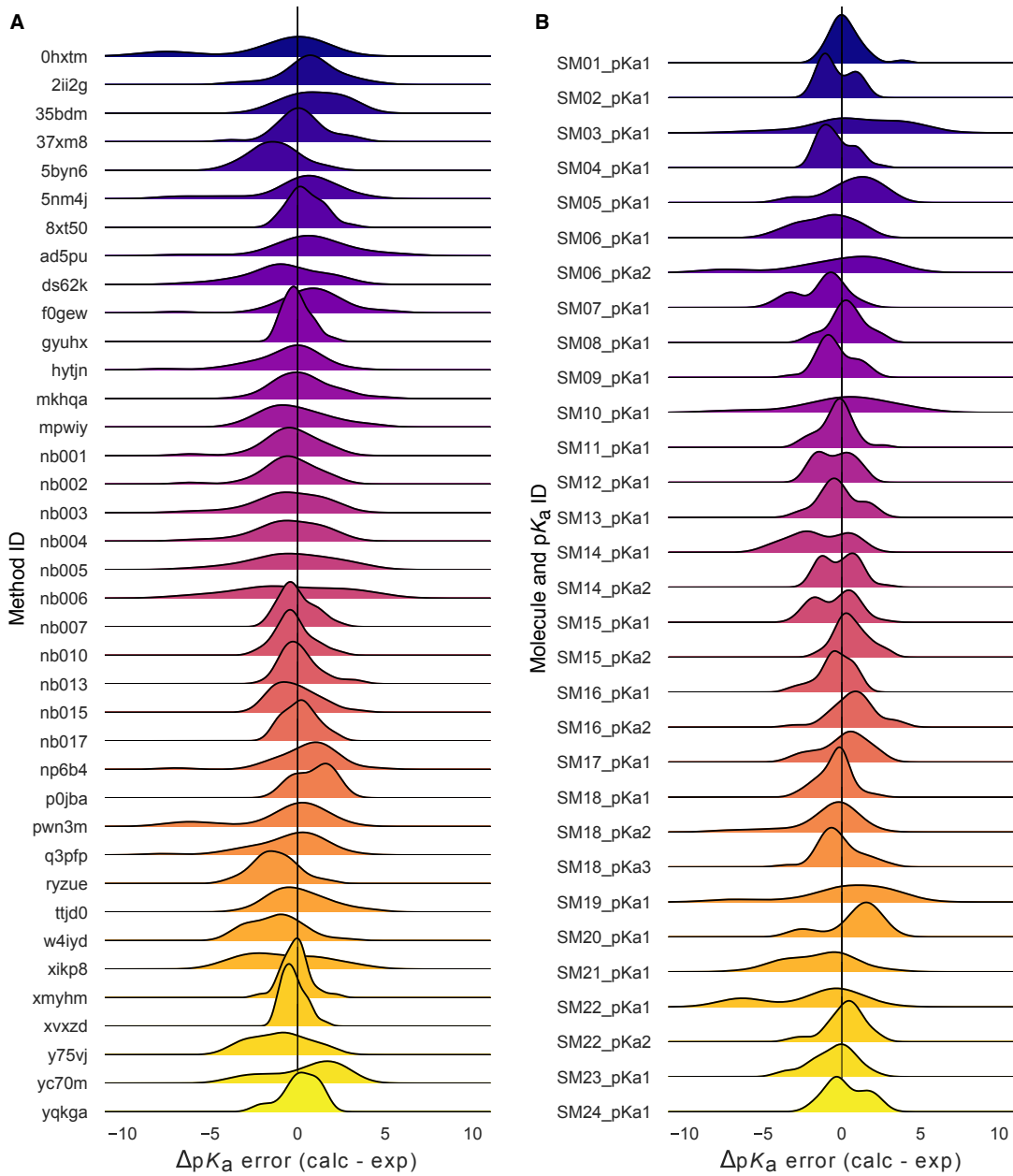


Figure 7. Macroscopic pK_a prediction error distribution plots show how prediction accuracy varies across methods and individual molecules. (A) pK_a prediction error distribution for each submission for all molecules according to Hungarian matching. (B) Error distribution for each SAMPL6 molecule for all prediction methods according to Hungarian matching. For multiprotic molecules, pK_a ID numbers (pKa1, pKa2, and pKa3) were assigned in the direction of increasing experimental pK_a value.

503 with the assumption that the 18 molecules have single titratable site is not the best approach. Instead analysis at the level of
504 macroscopic pK_a s is much more appropriate when a numerical matching scheme is the only option to evaluate predictions using
505 macroscopic experimental data.

506 For a subset of the molecules in the dataset of 8 molecules, dominant microstates were inferred from NMR experiments.
507 This dataset was extremely useful for guiding the assignment between experimental and predicted pK_a values based on mi-
508 crostates. In this section we present the performance evaluations of microscopic pK_a predictions for only the 8 compounds with
509 experimentally determined dominant microstates.

510 3.2.1 Microstate-based matching revealed errors masked by pK_a value-based matching between experimental 511 and predicted pK_a s

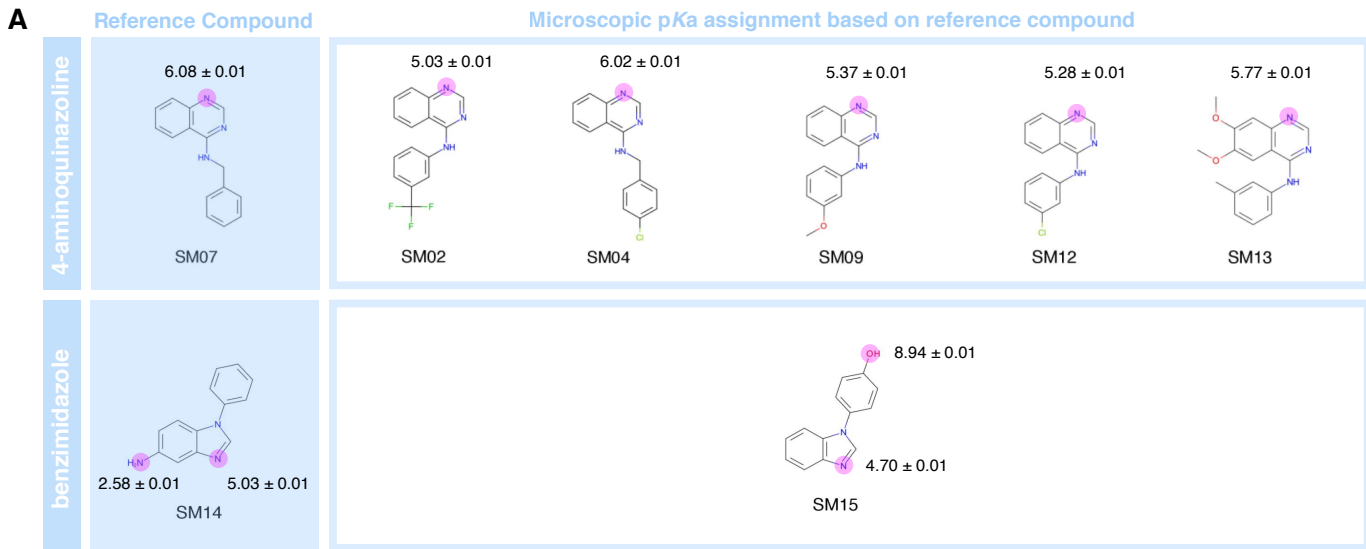
512 Comparing microscopic pK_a predictions directly to macroscopic experimental pK_a values with numerical matching can lead to
513 underestimation of errors. To demonstrate how numerical matching often masks the pK_a prediction errors we compared the
514 performance analysis done by Hungarian matching to microstate-based matching for 8 molecules presented in Fig. 8A. RMSE
515 calculated for microscopic pK_a predictions matched to experimental values via Hungarian matching is shown in Fig. 8B, while
516 Fig. 8C shows RMSE calculated via microstate-based matching. What is important to notice is that the Hungarian matching
517 leads to significantly lower RMSE compared to microstate-based matching. The reason is that the Hungarian matching assigns
518 experimental pK_a values to predicted pK_a values only based on the closeness of the numerical values, without consideration
519 of the relative population of microstates and microstate identities. Because of that a microscopic pK_a value that describes a
520 transition between very low population microstates (high energy tautomers) can be assigned to the experimental pK_a if it has
521 the closest pK_a value. This is not helpful, because in reality the microscopic pK_a s that influence the observable macroscopic pK_a
522 the most are the ones with higher populations (transitions between low energy tautomers).

523 The number of unmatched predicted microscopic pK_a s are shown in lower bar plots of Fig. 8B and C, to emphasize the large
524 number of microscopic pK_a predictions submitted by many methods. In the case of microscopic pK_a the number of unmatched
525 predictions do not indicate an error in the form of an extra predicted pK_a , because the spectrophotometric experiments do not
526 capture all microscopic pK_a s theoretically possible (transitions between all pairs of microstates that are 1 proton apart). pK_a s
527 of transitions to and from very high energy tautomers are very hard to measure by experimental methods, including the most
528 sensitive methods like NMR. The reason we plotted them was more to demonstrate how the increased number of prediction
529 value choices for Hungarian matching can lead to erroneously low RMSE values. We have also checked how often Hungarian
530 matching led to the correct matches between predicted and experimental pK_a in terms of the microstate pairs, i.e. how often the
531 microstate pair of the Hungarian match recapitulates the dominant microstate pair of the experiment. The overall accuracy of
532 correct microstate pair match was found to be low for SAMPL6 Challenge submission. Fig. S4 shows that for most methods the
533 predicted microstate pair selected by Hungarian match did not match experimentally determined microstate pair. This means
534 the lower RMSE results obtained from Hungarian matching are low for the wrong reason. Matching experimental and predicted
535 values on the basis of microstate IDs do not suffer from this problem.

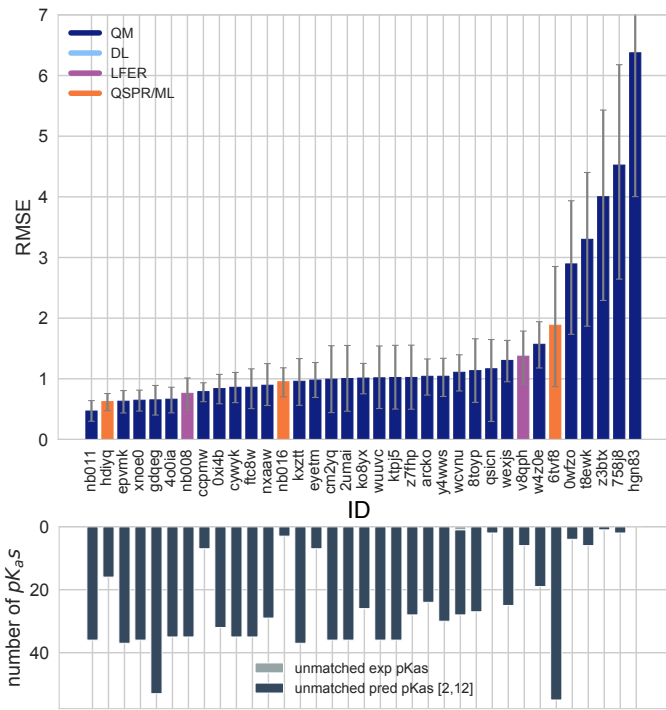
536 The disadvantage of the evaluation through microstate-based matching approach is that the conclusions in this section are
537 only about a subset of challenge compounds with limited diversity. This subset is composed of 6 molecules 4-aminoquinazoline
538 and 2 molecules with benzimidazole scaffolds, and a total of 10 pK_a values. The sequence of dominant microstates for SM07 and
539 SM14 were determined by NMR experiments directly [7], and dominant microstates of their derivatives were inferred taking them
540 as reference (Fig. 8). Although, we believe that microstate-based evaluation is more informative, the lack of a large experimental
541 dataset limits the conclusions to a very narrow chemical diversity.

542 3.2.2 Accuracy of pK_a predictions evaluated by microstate-based matching

543 Both accuracy and correlation based statistics were calculated for predicted microscopic pK_a values after microstate-based
544 matching. RMSE, MAE, ME, R^2 , and Kendall's Tau results of each method are shown in Fig. 8C and Fig. 9. A table of the calculated
545 statistics can be found in Table S4. Due to small number of data points in this set, correlation based statistics calculated shows
546 large uncertainty and provide less utility for distinguishing better performing methods. Therefore we focused more on accuracy
547 based metrics for the analysis of microscopic pK_a s than correlation based metrics. In terms of accuracy of microscopic pK_a
548 value, all three QSPR/ML based methods (*nb016* (MoKa), *hdijyq* (Simulations Plus), *6tvf8* (OE Gaussian Process)), three QM-based
549 methods (*nb011* (Jaguar), *ftc8w* (EC-RISM/MP2/cc-pVTZ-P2-q-noThiols-2par), *t8ewk* (COSMOlogic_FINE17)), and one LFER method
550 (*v8qph* (ACD/pKa GALAS)) achieved RMSE lower than 1 pK_a unit. The same 6 methods also have the lowest MAE.



B Hungarian matching



C Microstate-based matching

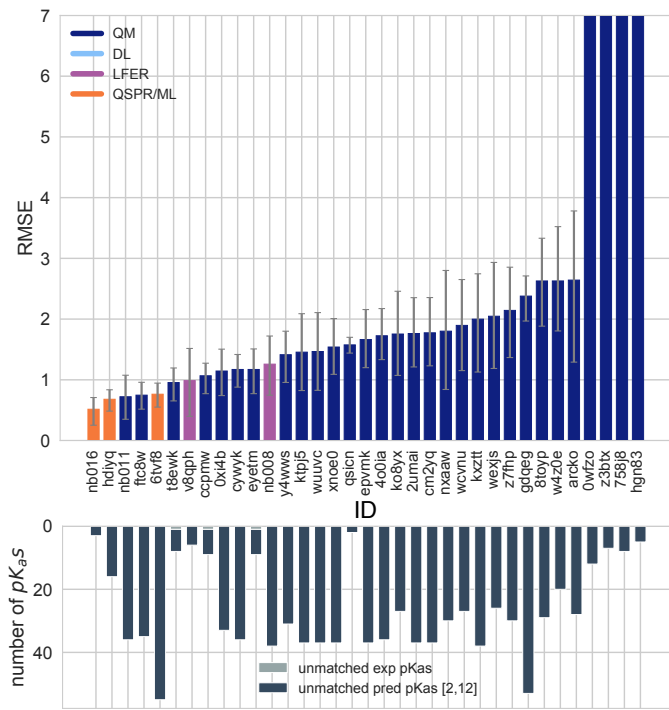


Figure 8. NMR determination of dominant microstates allowed in depth evaluation of microscopic pK_a predictions of 8 compounds.

A Dominant microstate sequence of two compounds (SM07 and SM14) were determined by NMR [7]. Based on these reference compounds dominant microstates of 6 other derivative compounds were inferred and experimental pK_a values were assigned to titratable groups with the assumption that only the dominant microstates have significant contributions to the experimentally observed pK_a . **B** RMSE vs. submission ID and unmatched pK_a vs. submission ID plots for the evaluation of microscopic pK_a predictions of 8 molecules by Hungarian matching to experimental macroscopic pK_a s. **C** RMSE vs. submission ID and unmatched pK_a vs. submission ID plots showing the evaluation of microscopic pK_a predictions of 8 molecules by microstate-based matching between predicted microscopic pK_{aS} and experimental macroscopic pK_a values. Submissions *Qwfzo*, *z3btx*, *758j8*, and *hgn83* have RMSE values bigger than 10 pK_a units which are beyond the y-axis limits of subplot **C** and **B**. RMSE is shown with error bars denoting 95% confidence intervals obtained by bootstrapping over challenge molecules. Lower bar plots show the number of unmatched experimental pK_{aS} (light grey, missing predictions) and the number of unmatched pK_a predictions (dark grey, extra predictions) for each method between pH 2 and 12. Submission IDs are summarized in Table 1.

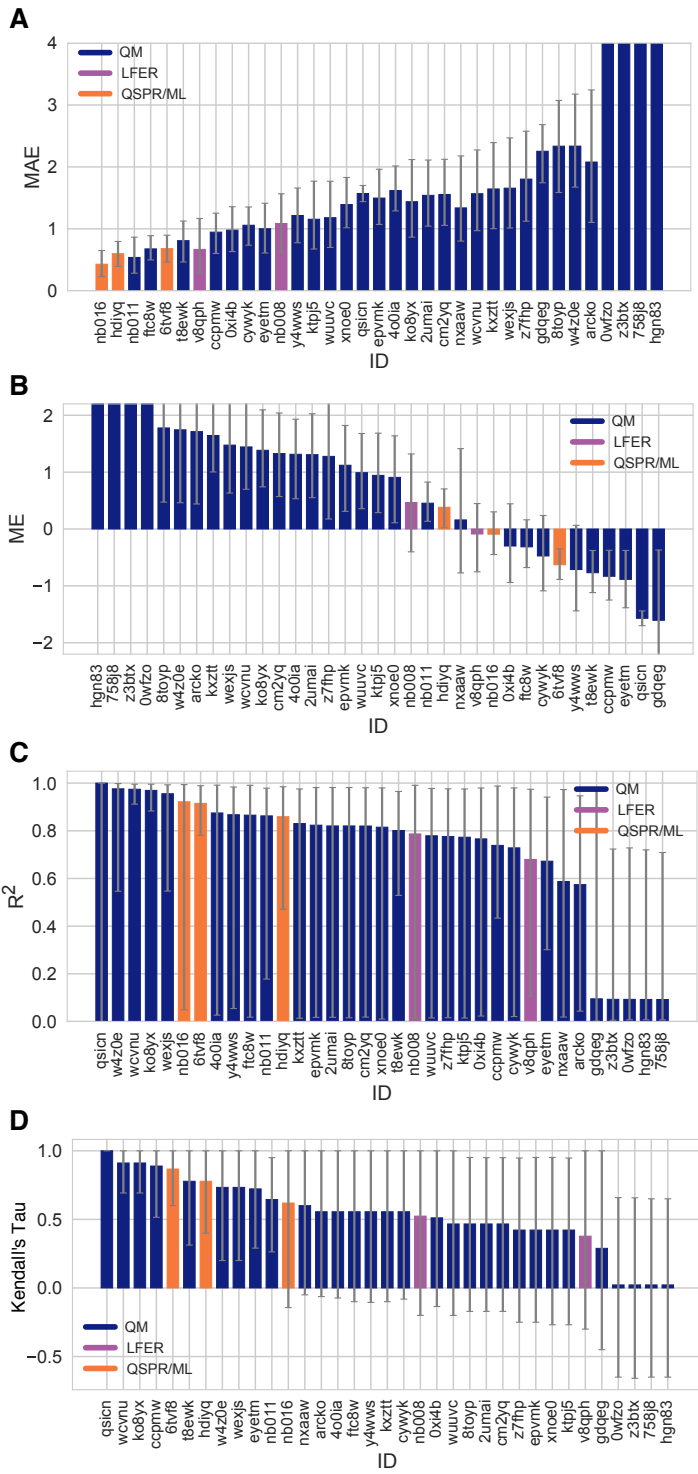


Figure 9. Additional performance statistics for microscopic pK_a predictions for 8 molecules with experimentally determined dominant microstates. Microstate-based matching was performed between experimental pK_a values and predicted microscopic pK_a values. Mean absolute error (MAE), mean error (ME), Pearson's R^2 , and Kendall's Rank Correlation Coefficient τ are shown, with error bars denoting 95% confidence intervals obtained by bootstrapping over challenge molecules. Methods are indicated by submission IDs. Submissions are colored by their method categories. Refer to Table 1 for submission IDs and method names. Submissions 0wfzo, z3btx, 758j8, and hgn83 have MAE and ME values bigger than 10 pK_a units which are beyond the y-axis limits of subplots A and B. A large number and wide variety of methods have a statistically indistinguishable performance based on correlation based statistic (C and D), in part because of the relatively small dynamic range the small size of the set of 8 molecules.

551 3.2.3 Evaluating microstate prediction accuracy of methods

552 For many computational chemistry approaches including structure based modeling of protein-ligand interactions, predicting
553 the ionization state and the exact position of protons is important to guide modeling. This is why in addition to being able to
554 predict pK_a values accurately, we need pK_a prediction methods to be able to capture microscopic protonation states accurately.
555 Even when the predicted pK_a value is very accurate, the predicted protonation site can be wrong. Therefore, we assessed if
556 methods participating the SAMPL6 pK_a Challenge were predicting correctly the sequence of dominant microstates, i.e. dominant
557 tautomers of each charge state observed between pH 2 and 12.

558 Analyze which state has lowest free energy for each charge group (The sequence of "experimentally visible states")

559 Dominant microstate prediction accuracy of microscopic pK_a prediction method are shown in Fig. 10. To extract the domi-
560 nant tautomers predicted for the sequence of ionization states of each method, first, relative free energy of microstates were
561 calculated at reference pH 0 [18]. Then to determine dominant microstate of each charge, we have selected the lowest energy
562 tautomer for each ionization states of the charges -1, 0, 1, and 2 (the charge range captured by NMR) experiments. Than pre-
563 dicted and experimental dominant microstates were compared for each charge to calculate the fraction of correctly predicted
564 dominant tautomers. This value is reported as the dominant microstate accuracy for all charges (Fig. 10A). Dominant microstate
565 prediction errors were present the methods participating in the SAMPL6 pK_a Challenge. 10 QM and 3 QSPR/ML methods did not
566 make any mistakes in dominant microstate predictions, although, they are expected to be making mistakes in the relative ratio
567 of tautomers (free energy difference between microstates) as reflected by pK_a value errors. While all the participating QSPR/ML
568 methods showed good performance in dominant microstate prediction, LFER and some QM methods made mistakes. Accuracy
569 of the prediction of the neutral dominant tautomers was perfect for all methods, except *qsicn* (Fig. 10B). But errors in predicting
570 the major tautomer of charge +1 was much more frequent. 22 out of 35 prediction sets made at least one error in prediction the
571 lowest energy tautomer with +1 charge. We didn't include ionization states with charges -1 and +2 in this assessment because
572 we had only one compound with these charges in the dataset. Never the less, dominant tautomer prediction errors seems to
573 be a bigger problem for charged tautomers than the neutral tautomer.

574 Experimental data of the sequence of dominant microstates was only available for 8 compounds. Therefore conclusions the
575 performance of methods in terms of dominant tautomer prediction are limited to this narrow chemical diversity (benzimid-
576 azole and 4-aminoquinazoline derivatives). We present this analysis as a prototype of how microscopic pK_a predictions should
577 be evaluated. To reach broad conclusions about which methods are better for capturing dominant microstates and ratios of
578 tautomers we hope that in the future more extensive evaluations can be mode with larger experimental datasets following the
579 strategy we are demonstrating here. Even if experimental microscopic pK_a measurement data is not available, experimental
580 dominant tautomer determinations are still informative for assessing prediction methods.

581 Focusing on dominant microstate sequence prediction accuracy from the perspective of molecules showed that major tau-
582 tomer of SM14 cationic form was the most frequently mispredicted one. Fig. 10 shows the dominant microstate prediction
583 accuracy calculated for individual molecules for charge states 0 and +1, averaged over all prediction methods. SM14, the
584 molecule that exhibits highest microstate prediction error, has two experimental pK_a values that were 2.4 pK_a units apart and
585 we suspect that could be a contributor to the difficulty of predicting microstates accurately. Other molecules are monoprotic
586 (4-aminoquinazolines) or their experimental pK_a values are very well separated (SM14, 4.2 pK_a units). It would be very interesting
587 to expand this assessment to a larger variety of drug-like molecules to discover for which structures tautomer predictions are
588 more accurate and for which structure computational predictions are not as reliable.

589 3.2.4 Consistently-well performing methods for microscopic pK_a predictions

590 To determine consistently top-performing methods for microscopic pK_a predictions we have determined different criteria than
591 macroscopic pK_a predictions: having perfect dominant microstate prediction accuracy, unmatched pK_a count of 0, and ranking
592 in the top 10 according RMSE and MAE. Correlation based statistics were not found to have utility for discriminating perfor-
593 mance due to large uncertainties in this statistics for a small dataset of 10 pK_a values. Unmatched predicted pK_a count was
594 also not a consideration, since experimental data was only informative for the pK_a between dominant microstates and did not
595 capture the all possible theoretical transitions between microstate pairs. Table 3 reports six methods that have consistent well
596 performance according to many metrics, although evaluated only for the 8 molecule set due to limitations of the experimen-
597 tal dataset. Six methods were divided evenly between methods of QSPR/ML category and QM category. *nb016* (MoKa), *hdijyq*
598 (*Simulations Plus*), and *6tvf8* (OE Gaussian Process) were QSPR and ML based methods that performed well. *nb011* (Jaguar),
599 *0xi4b*(EC-RISM/B3LYP/6-311+G(d,p)-P2-phi-noThiols-2par), and *cwyk* (EC-RISM/B3LYP/6-311+G(d,p)-P2-phi-noThiols-2par) were
600 QM predictions with linear empirical corrections with good performance with microscopic pK_a predictions.

Simulations Plus pK_a prediction method is the only method that appeared to be consistently well performing in both the assessment for macroscopic and microscopic pK_a prediction (and hdiyq). However it is worth noting that two methods that were in consistently top-performing methods list for macroscopic pK_a predictions lacked equivalent submissions of their underlying microscopic pK_a predictions and therefore could not be evaluated at the microstate level. These methods were (ACD/Classic pKa) and xvxdz(DSD-BLYP-D3(BJ)/def2-TZVPD//PBEh-3c[DCOSMO-RS] + RRHO(GFN-xTB[GBSA]) + Gsolv(COSMO-RS[TZVPD]) and linear fit).

Table 3. Top performing methods for microscopic pK_a predictions based on consistent ranking within the Top 10 according to various statistical metrics calculated for 8 molecule dataset. Performance statistics are provided as mean and 95% confidence intervals. Submissions that rank in the Top 10 according to RMSE and MAE, and have perfect dominant microstate prediction accuracy were selected as consistently well-performing methods. Correlation-based statistics (R^2 , and Kendall's Tau), although reported in the table, were excluded from the statistics used for determining top-performing methods. This was because correlation-based statistics were not very discriminating due to narrow dynamic range and the small number of data points in the 8 molecule dataset with NMR-determined dominant microstates.

Submission ID	Method Name	Dominant Microstate Accuracy	RMSE	MAE	R ²	Kendall's Tau	Unmatched Exp. pK _a Count	Unmatched Pred. pK _a Count [2,12]
nb016	MoKa	1.0 [1.0, 1.0]	0.52 [0.25, 0.71]	0.43 [0.23, 0.65]	0.92 [0.05, 0.99]	0.62 [-0.14, 1.00]	0	3
hdiyq	S+pKa	1.0 [1.0, 1.0]	0.68 [0.49, 0.83]	0.60 [0.39, 0.80]	0.86 [0.47, 0.98]	0.78 [0.40, 1.00]	0	16
nb011	Jaguar	1.0 [1.0, 1.0]	0.72 [0.35, 1.07]	0.54 [0.28, 0.86]	0.86 [0.18, 0.98]	0.64 [0.26, 0.95]	0	36
6tvf8	OE Gaussian Process	1.0 [1.0, 1.0]	0.76 [0.55, 0.95]	0.68 [0.46, 0.90]	0.92 [0.78, 0.99]	0.87 [0.6, 1.00]	0	55
Oxi4b	EC-RISM/B3LYP/6-311+G(d,p)-P3NI-phi-noThiols-2par	1.0 [1.0, 1.0]	1.15 [0.75, 1.50]	0.98 [0.63, 1.36]	0.77 [0.02, 0.98]	0.51 [-0.14, 1.00]	0	33
cywyk	EC-RISM/B3LYP/6-311+G(d,p)-P2-phi-noThiols-2par	1.0 [1.0, 1.0]	1.17 [0.88, 1.41]	1.06 [0.74, 1.35]	0.73 [0.02, 0.98]	0.56 [-0.08, 1.00]	0	36

3.3 How do pK_a prediction errors impact protein-ligand binding affinity predictions?

Physical modeling methods for predicting protein-ligand binding affinities rely on pK_a predictions for modeling the protein and the ligand. As SAMPL6 pK_a Challenge only focused on small molecule pK_a prediction we will ignore the protonation state effects of the protein for now. Many affinity prediction methods such as docking, MM/PBSA, MM/GBSA, absolute or alchemical relative free energy calculation methods predict the affinity of a fixed protonation state of the ligand to a receptor. These models strictly depend on pK_a predictions for determining possible protonation states of the ligand in aqueous environment and in protein complex, as well as the free energy penalty to reach those states [3]. Accuracy of pK_a predictions can become a limitation for the performance of physical models that try to capture molecular association.

In terms of the ligand protonation states, there are two ways in which the pK_a prediction errors can influence the prediction accuracy for protein-ligand binding free energies as depicted in Fig. 11. First scenario is when ligand is present in aqueous solution in multiple protonation states (Fig. 11A). When only the minor aqueous protonation state contributes to protein-ligand complex formation, overall binding free energy (ΔG_{bind}) needs to be calculated as the sum of binding affinity of the minor state and the protonation penalty of that state (ΔG_{prot}). ΔG_{prot} is a function of pH and pK_a. A 1 unit of error in pK_a value would lead to 1.36 kcal/mol error in overall binding affinity, if the protonation state with the minor population binds the protein. The equations in Fig. 11A show the calculation of overall affinity.

In addition to multiple protonation states being present in the aqueous environment, multiple charge states can contribute to complex formation (Fig. 11B). Then, overall free energy of binding needs to include a Multiple Protonation States Correction (MPSC) term (ΔG_{corr}). MPSC is a function of pH, aqueous pK_a of the ligand, and the difference between the binding free energy of charged and neutral species ($\Delta G_{bind}^C - \Delta G_{bind}^N$) as shown in Fig. 11B.

Using Equation 9 we can model the true MPSC (ΔG_{corr}) value with respect to the difference between pH and the pK_a of the ligand, to see when this value has significant impact to overall binding free energy. In Fig. 12, true MPSC value that needs to be added to the ΔG_{bind}^N is shown for ligands with varying binding affinity difference between protonation states ($\Delta\Delta G = \Delta G_{bind}^C - \Delta G_{bind}^N$) and varying free energy of binding difference between the protonation states. Fig. 12A shows the simulation of a case where for a monoprotic base which has a charged state with lower affinity than the neutral state. Solid lines show the true correction. In situations where pK_a is lower than pH, correction factor disappears as the ligand fully populates the neutral state ($\Delta G_{bind} = \Delta G_{bind}^N$). As the pK_a value gets larger than the pH, the charged state is populated more and ΔG_{corr} value increases to approach significant $\Delta\Delta G$. What is interesting to note is the pH-pK_a range that ΔG_{corr} changes. It is often assumed that for a

basic ligand if pK_a of a ligand is more than 2 units higher than the pH, then only 1% of the population is in neutral state and it is safe to approximate the overall binding affinity with ΔG_{bind}^C only. Based on the relative free energy difference between ligand this assumption is not always correct. As seen in Fig. 12A, responsive region of ΔG_{corr} can span 3 pH units for a system with $\Delta\Delta G = 1 \text{ kcal/mol}$ or 5 pH units for a system with $\Delta\Delta G = 4 \text{ kcal/mol}$. This highlights that the range of pK_a values that impact binding affinity predictions is wider than previously appreciated. Molecules with pK_a s several units away from the physiological pH can still impact the overall binding affinity significantly due to MPSC.

Despite the need to capture the contributions of multiple protonations states by including MPSC in binding affinity calculations, inaccurate pK_a predictions can lead to errors in ΔG_{corr} and overall free energy of binding prediction. In Fig. 12A dashed lines show predicted ΔG_{corr} based on pK_a error of -1 units. We have chosen a pK_a error of 1 units as this is the average performance expected from the pK_a prediction methods based on the SAMPL6 Challenge. Underestimated pK_a causes underestimated ΔG_{corr} and overestimated affinities for a varying range of pH - pK_a values depending on binding affinity difference between protonation states($\Delta\Delta G$). In Fig. 12B dashed lines shows how the magnitude of the absolute error caused by calculating ΔG_{corr} with an inaccurate pK_a varies with respect to pH. Different colored lines show simulated results with varying binding affinity difference between protonation states. For a system whose charged state has lower affinity than the neutral state ($\Delta\Delta G = 2 \text{ kcal/mol}$), the absolute error caused by underestimated pK_a by 1 units only can be up to 0.9 kcal/mol. For a system whose charged state has even lower affinity than the neutral state ($\Delta\Delta G = 4 \text{ kcal/mol}$), the absolute error caused by underestimated pK_a by 1 units only can be up to 1.2 kcal/mol. The magnitude of errors contributing to overall binding affinity are too large to be neglected. Improving the accuracy of small molecule pK_a prediction methods can help to minimize the error in predicted MPSC.

With the current level of pK_a prediction accuracy as observed in SAMPL6 Challenge, is it advantageous to include MPSC in affinity predictions that may be include errors caused by pK_a predictions? We provide a comparison of the two choices to answer this question: (1) Neglecting MPSC completely and assuming overall binding affinity is captured by ΔG_{bind}^N , (2) including MPSC with potential error in overall affinity calculation. The magnitude of error caused by Choice 1 (ignoring MPSC) is depicted as solid line in Fig. 12B and the magnitude of error caused by MPSC computed with inaccurate pK_a is depicted as dashed lines. What is the best strategy? Error due to choice 1 is always larger than error due to choice 2 for all pH- pK_a values. In this scenario including MPSC improves overall binding affinity prediction. The error caused my inaccurate pK_a is smaller than the error caused by neglecting MPSC.

The same question about whether or not an MPSC calculated based on an inaccurate pK_a should be included in binding affinity predictions can be asked for different circumstances underestimated or overestimated pK_a values, charged states with higher or lower affinities than the neutral states. We tried to capture these 4 circumstances in four quadrants of Fig. 12. In the case of overestimated pK_a values (Fig. 12E-H) it can be seen that for the most of the pH- pK_a range it is more advantageous to include the predicted MPSC in affinity calculations, except a smaller window where the opposite choice would be more advantageous. For instance, for the system with $\Delta\Delta G = 2 \text{ kcal/mol}$ and overestimated pK_a (Fig. 12E) for the pH- pK_a region between -0.5 and 2, including predicted ΔG_{corr} causes more error than ignoring MPSC.

In reality we do not know the exact magnitude or the direction of the error of our predicted pK_a , therefore using simulated MPSC error plots to make the decision about when to include MPSC in binding affinity predictions is not possible. But based on the analysis of extreme cases, with 1 unit of pK_a error including MPSC correction is more often than not helpful in imporving binding affinity predictions. The detrimental effect of pK_a inaccuracy is still significant, however, future improvements in pK_a prediction methods can improve the accuracy of MPSC and binding affinity predictions of ligands which have multiple protonation states that contribute to aqueous or complex populations. Achieving pK_a value prediction accuracy of 0.5 units would significantly help the binding affinity models to incorporate more accurate MPSC terms.

3.4 Take-away lessons from SAMPL6 pK_a Challenge

SAMPL6 pK_a Challenge showed that in general pK_a prediction performance of computational methods are lower than expected for drug-like molecules. Multiple titration sutes, tautomerization, frequent presence of heterocycles and extended conjugation patterns, as well as high number of rotatable bonds, and the possibility of intramolecular hydrogen bonds are factors that complicate pK_a prediction of drug-like molecules. For macroscopic pK_a predictions have not yet reached experimental accuracy. Inter-method variability of macroscopic pK_a measurements can be around 0.5 pK_a units [14]. There was not a single method in SAMPL6 Challenge that achieved RMSE around 0.5 or lower for macropscoptic pK_a predictions for the 24 molecule set of kinase inhibitor fragment-like molecules. Lower RMSE values were observed in the microscopic pK_a evaluation section of this study for some methods however the 8 molecule set used for that analysis poses a very limited dataset to reach conclusions about general expectations for drug-like molecules.

684 As the majority of experimental data was in the form of macroscopic pK_a values, we had to adopt a numerical matching
685 algorithm (Hungarian matching) to pair predicted and experimental values to calculate performance statistics of macroscopic
686 pK_a predictions. Accuracy, correlation, and extra/missing pK_a prediction counts were the main metrics for macroscopic pK_a
687 evaluations. An RMSE range of 0.7 to 3.2 pK_a units. Only five methods achieved RMSE between 0.7-1 pK_a units, while an RMSE
688 between 1.5-3 log units was observed for the majority of methods. All four methods of LFER category and three out of 5 QSPR/ML
689 methods achieved RMSE less than 1.5 pK_a units. All the QM methods that achieved this level of performance included linear
690 empirical corrections to rescale and unbias their pK_a predictions.

691 Based on consideration of multiple error metrics, we compiled a short list of consistently-well performing methods for macroscopic
692 pK_a evaluations. Two methods from QM+LEC methods, one QSPR/ML, two empirical methods achieved consistent per-
693 formance according to many metrics. The common features of the two empirical methods were their large training sets (16000-
694 17000 compounds) and being commercial prediction models.

695 There were four submissions of QM-based methods that utilized COSMO-RS implicit solvation model. It was interesting
696 that while three of these achieved the lowest RMSE among QM-based methods (*xvxzd*, *yqkga*, and *8xt50*) [32] and one of them
697 showed the highest RMSE (*0hxtm* (COSMOtherm_FINE17)) in SAMPL6 Challenge macroscopic pK_a predictions. Comparison of
698 these methods indicates that capturing conformational ensemble of microstates, high level QM calculations, and RRHO cor-
699 rections were factors contributing to better macroscopic pK_a predictions. Linear empirical corrections applied QM calculations
700 impored results, especially when the linear correction is calibrated for an experimental dataset using the same level of theory
701 ast the deprotonation free energy predictions (as in *xvxzd*). This challenge also points to the advantage of COSMO-RS solvation
702 approach compared to other implicit solvent models.

703 Evaluation of macroscopic pK_a prediction accuracy of individual molecules on average considering all the predictions in
704 SAMPL6 Challenge provided insight into which molecules posed greater difficulty for pK_a predictions. pK_a prediction errors
705 were higher for compounds with sulfur-containing heterocycles, iodo, and bromo groups. This trend was also conserved when
706 only QM-based methods were analyzed. SAMPL6 pK_a dataset consisted of only 24 small molecules which limited our ability
707 to statistically confirm this conclusion, however, we believe it is worth reporting molecular features that coincided with larger
708 errors even if we can not evaluate the driving reason for these failures.

709 Utilizing a numerical matching algorithm to pair experimental and predicted macroscopic pK_a values was a necessity, how-
710 ever, this approach did not capture all aspects of prediction errors. Computing the number of missing or extra pK_a predictions
711 remaining after Hungarian matching, provided a window of observing macroscopic pK_a prediction errors such as number of
712 macroscopic transitions or ionization states expected in a pH interval. In pK_a evaluation studies it is very typical to just focus
713 on pK_a value errors evaluated after matching, and to ignore pK_a prediction errors that the matching protocol can not capture.
714 SAMPL6 pK_a Challenge results showed sporadic presence of missing pK_a predictions and very frequent case of extra pK_a predic-
715 tions. Both indicates failures to capture the correct sequence of ionizations states. The traditional way of evaluating pK_a s that
716 only focuses on the pK_a value error after some sort of numerical match between predictions and experimental values may have
717 motivated these types of errors as there would be no penalty for missing a macroscopic deprotonation and predicting an extra
718 one. This problem does not seem to be specific to any method category.

719 Factors to consider when deciding which pK_a prediction method to consider? -license -how expensive is the calculation -
720 macroscopic pK_a value accuracy -macrostate number accuracy -microscopic pK_a value accuracy - microstate accuracy - tautomer
721 ratio, correct relative free energy between tautomers

722 Errors computed by microstate-based matching are larger compared to numerical matching algorithms. Microscopic pK_a
723 analysis with numerical matching algorithms may mask errors due to higher number of guesses made.

724 Due to the size of the experimental datasets evaluation of macroscopic pK_a prediction carried more weight in assessing
725 performance of computational predictions, although microscopic pK_a evaluation can provide much more in depth analysis and
726 can be more informative about capturing reasons for failure.

727 3.5 Suggestions for future challenge design and evaluation of pK_a predictions

728 When the experimental data is in the form of macroscopic pK_a values, the best way to evaluate computational predictions is in the
729 level of predicted macroscopic pK_a s. Microscopic pK_a predictions can be converted to macroscopic pK_a predictions. Discussion
730 of matching problem betwene experimental and predicted values. Difficulty of assessing predicted pK_a s using experimental
731 data: matching problem Explain rationale behind how we analyze the data and determine success/failure.

732 In the SAMPL6 pK_a Challenge there wasn't a requirement that prediction sets should report predictions for all compounds.
733 Some participants reported predictions for only a subset of compounds which may lead these methods to look more accurate

734 than others, due to missing predictions. It would have been a better choice to require submissions for whole sets for better
735 comparison of method performance.

736 **Discuss what can be done to further improve future challenges**

737 How can we maximize what we learn? What should we have people predict? How should we select compounds / measure
738 pKas?

739 **Suggestions about challenge construction**

740 Future challenge direction Challenge path: predict pKas, give people pKas to predict logDs on same molecules, then predict
741 for new set of compounds logDs without provided pKas.

742 Enumeration of protonation states before predictions (which states does one need to consider?)

743 **Suggestions about challenge analysis**

744 NMR experimental techniques could be used to validate microstate information in future challenges

745 Reporting microscopic pKa predictions with charges, microstate free energies is better Experimental dataset with microstate
746 information is more helpful.

747 What can be done to further improve future challenges How can we maximize what we learn? What should we have people
748 predict? How should we select compounds / measure pKas? NMR experimental techniques could be used to validate microstate
749 information in future challenges

750 Suggestions about challenge construction Enumeration of protonation states before predictions (which states does one need
751 to consider?) Suggestions about challenge analysis

752 Submitting pKa predictions in terms of relative free energy of microstates, from which both microscopic and macroscopic
753 pKas and fractional populations of states at and pH can be calculated. Explicit hydrogen mol2 format can be used to capture
754 individual tautomers

755 Capture computing costs in terms of average compute hours per molecule

756 **4 Conclusion**

757 **5 Code and data availability**

- 758 • SAMPL6 pK_a challenge instructions, submissions, experimental data and analysis is available at
<https://github.com/samplchallenges/SAMPL6>

759 **6 Overview of supplementary information**

760 Contents of the Supplementary Information:

- 761 • TABLE S1: SMILES and InChI identifiers of SAMPL6 pK_a Challenge molecules.
- 762 • TABLE S2: Evaluation statistics calculated for all macroscopic pK_a prediction submissions based on Hungarian match for
24 molecules.
- 763 • TABLE S3: Evaluation statistics calculated for all microscopic pK_a prediction submissions based on Hungarian match for 8
molecules with NMR data.
- 764 • TABLE S4: Evaluation statistics calculated for all microscopic pK_a prediction submissions based on microstate match for 8
molecules with NMR data.
- 765 • FIGURE S1: Dominant microstates of 8 molecules were determined based on NMR measurements.
- 766 • FIGURE S2: MAE of macroscopic pK_a predictions of each molecule did not show any significant correlation with any molec-
ular descriptor.
- 767 • FIGURE S3: The value of macroscopic pK_a was not a factor affecting prediction error seen in SAMPL6 Challenge according
to the analysis with Hungarian matching.
- 768 • FIGURE S4: There was low agreement between experimental dominant microstate pairs and the predicted microstate pairs
selected by Hungarian algorithm for microscopic pK_a predictions.

775 Extra files included in *SAMPL6-supplementary-documents.tar.gz*:

- 776 • SAMPL6-pKa-chemical-identifiers-table.csv
- 777 • macroscopic-pKa-statistics-24mol-hungarian-match.csv
- 778 • microscopic-pKa-statistics-8mol-hungarian-match-table.csv

- 779 • microscopic-pKa-statistics-8mol-microstate-match-table.csv
780 • experimental-microstates-of-8mol-based-on-NMR.csv
781 • enumerate-microstates-with-Epik-and-OpenEye-QUACPAC.ipynb
782 • molecule_ID_and_SMILES.csv

783 **7 Author Contributions**

784 Conceptualization, MI, JDC, CB, DLM ; Methodology, MI, JDC ; Software, MI, AR, ASR ; Formal Analysis, MI, ASR, AR ; Investigation,
785 MI ; Resources, JDC; Data Curation, MI ; Writing-Original Draft, MI, JDC; Writing - Review and Editing, MI, ASR, AR, CB, DLM, JDC;
786 Visualization, MI, AR ; Supervision, JDC, DLM, CB, ASR ; Project Administration, MI ; Funding Acquisition, JDC, DLM.

787 **8 Acknowledgments**

788 Complete acknowledgments section. Caitlin Bannan for guidance on working microstate definition for the challenge, Thomas Fox for
MoKa reference calculations, Kiril Lanevskij for hungarian algorithm

789 MI, ASR, and JDC acknowledge support from the Sloan Kettering Institute. JDC acknowledges support from NIH grant P30
790 CA008748. MI acknowledges Doris J. Hutchinson Fellowship. We thank Brad Sherborne for his valuable insights at the conception
791 of the pK_a challenge and connecting us with Timothy Rhodes and Dorothy Levorse who were able to provide resources and
792 expertise for experimental measurements performed at MRL. We acknowledge Paul Czodrowski who provided feedback on
793 multiple stages of this work: challenge construction, purchasable compound selection and manuscript. MI, ASR, AR and JDC are
794 grateful to OpenEye Scientific for providing a free academic software license for use in this work.

795 Mike Chui

796 **9 Disclosures**

797 JDC is a member of the Scientific Advisory Board for Schrödinger, LLC. DLM is a member of the Scientific Advisory Board of
798 OpenEye Scientific Software.

799 Table ref: [20, 21, 23, 24, 26] trial: [], +, -, *, #, \m

800 **References**

- 801 [1] **Manallack DT**, Prankerd RJ, Yuriev E, Oprea TI, Chalmers DK. The Significance of Acid/Base Properties in Drug Discovery. *Chem Soc Rev.* 2013; 42(2):485–496. doi: [10.1039/C2CS35348B](https://doi.org/10.1039/C2CS35348B).
- 803 [2] **Manallack DT**, Prankerd RJ, Nassta GC, Ursu O, Oprea TI, Chalmers DK. A Chemogenomic Analysis of Ionization Constants-Implications for
804 Drug Discovery. *ChemMedChem*. 2013 Feb; 8(2):242–255. doi: [10.1002/cmdc.201200507](https://doi.org/10.1002/cmdc.201200507).
- 805 [3] **de Oliveira C**, Yu HS, Chen W, Abel R, Wang L. Rigorous Free Energy Perturbation Approach to Estimating Relative Binding Affinities
806 between Ligands with Multiple Protonation and Tautomeric States. *Journal of Chemical Theory and Computation*. 2019 Jan; 15(1):424–435.
807 doi: [10.1021/acs.jctc.8b00826](https://doi.org/10.1021/acs.jctc.8b00826).
- 808 [4] **Darvey IG**. The Assignment of pKa Values to Functional Groups in Amino Acids. *Biochemical Education*. 1995 Apr; 23(2):80–82. doi:
809 [10.1016/0307-4412\(94\)00150-N](https://doi.org/10.1016/0307-4412(94)00150-N).
- 810 [5] **Bodner GM**. Assigning the pKa's of Polyprotic Acids. *Journal of Chemical Education*. 1986 Mar; 63(3):246. doi: [10.1021/ed063p246](https://doi.org/10.1021/ed063p246).
- 811 [6] **Murray R**. Microscopic Equilibria. *Analytical Chemistry*. 1995 Aug; p. 1.
- 812 [7] **İşik M**, Levorse D, Rustenburg AS, Ndukwe IE, Wang H, Wang X, Reibarkh M, Martin GE, Makarov AA, Mobley DL, Rhodes T, Chodera JD.
813 pKa Measurements for the SAMPL6 Prediction Challenge for a Set of Kinase Inhibitor-like Fragments. *Journal of Computer-Aided Molecular
814 Design*. 2018 Oct; 32(10):1117–1138. doi: [10.1007/s10822-018-0168-0](https://doi.org/10.1007/s10822-018-0168-0).
- 815 [8] **Selwa E**, Kenney IM, Beckstein O, Iorga BI. SAMPL6: Calculation of Macroscopic pKa Values from Ab Initio Quantum Mechanical Free
816 Energies. *Journal of Computer-Aided Molecular Design*. 2018 Oct; 32(10):1203–1216. doi: [10.1007/s10822-018-0138-6](https://doi.org/10.1007/s10822-018-0138-6).
- 817 [9] **Pickard FC**, König G, Tofoleanu F, Lee J, Simonett AC, Shao Y, Ponder JW, Brooks BR. Blind Prediction of Distribution in the SAMPL5
818 Challenge with QM Based Protomer and pK a Corrections. *Journal of Computer-Aided Molecular Design*. 2016 Nov; 30(11):1087–1100. doi:
819 [10.1007/s10822-016-9955-7](https://doi.org/10.1007/s10822-016-9955-7).

- 820 [10] **Bannan CC**, Mobley DL, Skillman AG. SAMPL6 Challenge Results from \$\$pK_a\$\$ Predictions Based on a General Gaussian Process Model.
821 Journal of Computer-Aided Molecular Design. 2018 Oct; 32(10):1165–1177. doi: [10.1007/s10822-018-0169-z](https://doi.org/10.1007/s10822-018-0169-z).
- 822 [11] **Işık M**, Levorse D, Mobley DL, Rhodes T, Chodera JD. Octanol–Water Partition Coefficient Measurements for the SAMPL6 Blind Prediction
823 Challenge. Journal of Computer-Aided Molecular Design. 2020 Apr; 34(4):405–420. doi: [10.1007/s10822-019-00271-3](https://doi.org/10.1007/s10822-019-00271-3).
- 824 [12] **Işık M**, Bergazin TD, Fox T, Rizzi A, Chodera JD, Mobley DL. Assessing the Accuracy of Octanol–Water Partition Coefficient Predictions in the
825 SAMPL6 Part II Log P Challenge. Journal of Computer-Aided Molecular Design. 2020 Apr; 34(4):335–370. doi: [10.1007/s10822-020-00295-0](https://doi.org/10.1007/s10822-020-00295-0).
- 826 [13] Special Issue: SAMPL6 (Statistical Assessment of the Modeling of Proteins and Ligands); October 2018. Volume 32, Issue 10. Journal of
827 Computer-Aided Molecular Design.
- 828 [14] **Fraczkiewicz R**. In Silico Prediction of Ionization. In: *Reference Module in Chemistry, Molecular Sciences and Chemical Engineering* Elsevier;
829 2013. doi: [10.1016/B978-0-12-409547-2.02610-X](https://doi.org/10.1016/B978-0-12-409547-2.02610-X).
- 830 [15] **Kuhn HW**. The Hungarian Method for the Assignment Problem. Naval Research Logistics Quarterly. 1955 Mar; 2(1-2):83–97. doi:
831 [10.1002/nav.3800020109](https://doi.org/10.1002/nav.3800020109).
- 832 [16] **Munkres J**. Algorithms for the Assignment and Transportation Problems. J SIAM. 1957 Mar; 5(1):32–28.
- 833 [17] SciPy v1.3.1, Linear Sum Assignment Documentation; Sep 27, 2019. The SciPy community. https://docs.scipy.org/doc/scipy-1.3.1/reference/generated/scipy.optimize.linear_sum_assignment.html.
- 835 [18] **Gunner MR**, Murakami T, Rustenburg AS, Işık M, Chodera JD. Standard State Free Energies, Not pKas, Are Ideal for Describing Small
836 Molecule Protonation and Tautomeric States. Journal of Computer-Aided Molecular Design. 2020 May; 34(5):561–573. doi: [10.1007/s10822-020-00280-7](https://doi.org/10.1007/s10822-020-00280-7).
- 838 [19] OpenEye pKa Prospector;. OpenEye Scientific Software, Santa Fe, NM. Accessed on Jan 23, 2018. <https://www.eyesopen.com/pka-prospector>.
- 839 [20] ACD/pKa GALAS (ACD/Percepta Kernel v1.6);. Advanced Chemistry Development, Inc., Toronto, ON, Canada, 2018. <https://www.acdlabs.com/products/percepta/predictors/pKa/>.
- 841 [21] ACD/pKa Classic (ACD/Percepta Kernel v1.6);. Advanced Chemistry Development, Inc., Toronto, ON, Canada, 2018. <https://www.acdlabs.com/products/percepta/predictors/pKa/>.
- 843 [22] **Shelley JC**, Cholleti A, Frye LL, Greenwood JR, Timlin MR, Uchimaya M. Epik: A Software Program for pK a Prediction and Protonation State
844 Generation for Drug-like Molecules. Journal of Computer-Aided Molecular Design. 2007 Dec; 21(12):681–691. doi: [10.1007/s10822-007-9133-z](https://doi.org/10.1007/s10822-007-9133-z).
- 846 [23] Simulations Plus ADMET Predictor v8.5;. Simulations Plus, Lancaster, CA, 2018. <https://www.simulations-plus.com/software/admetpredictor/physicochemical-biopharmaceutical/>.
- 848 [24] Chemicalize v18.23 (ChemAxon MarvinSketch v18.23);. ChemAxon, Budapest, Hungary, 2018. <https://docs.chemaxon.com/display/docs/pKa+Plugin>.
- 850 [25] **Milletti F**, Storchi L, Sforza G, Cruciani G. New and Original p K_a Prediction Method Using Grid Molecular Interaction Fields. Journal of
851 Chemical Information and Modeling. 2007 Nov; 47(6):2172–2181. doi: [10.1021/ci700018y](https://doi.org/10.1021/ci700018y).
- 852 [26] MoKa;. Molecular Discovery, Hertfordshire, UK, 2018. <https://www.moldiscovery.com/software/moka/>.
- 853 [27] **Zeng Q**, Jones MR, Brooks BR. Absolute and Relative pKa Predictions via a DFT Approach Applied to the SAMPL6 Blind Challenge. Journal
854 of Computer-Aided Molecular Design. 2018 Oct; 32(10):1179–1189. doi: [10.1007/s10822-018-0150-x](https://doi.org/10.1007/s10822-018-0150-x).
- 855 [28] **Bochevarov AD**, Harder E, Hughes TF, Greenwood JR, Braden DA, Philipp DM, Rinaldo D, Halls MD, Zhang J, Friesner RA. Jaguar: A High-
856 Performance Quantum Chemistry Software Program with Strengths in Life and Materials Sciences. International Journal of Quantum
857 Chemistry. 2013 Sep; 113(18):2110–2142. doi: [10.1002/qua.24481](https://doi.org/10.1002/qua.24481).
- 858 [29] **Tielker N**, Eberlein L, Güssregen S, Kast SM. The SAMPL6 Challenge on Predicting Aqueous pKa Values from EC-RISM Theory. Journal of
859 Computer-Aided Molecular Design. 2018 Oct; 32(10):1151–1163. doi: [10.1007/s10822-018-0140-z](https://doi.org/10.1007/s10822-018-0140-z).
- 860 [30] **Klamt A**, Eckert F, Diedenhofen M, Beck ME. First Principles Calculations of Aqueous p K_a Values for Organic and Inorganic Acids Using
861 COSMO-RS Reveal an Inconsistency in the Slope of the p K_a Scale. The Journal of Physical Chemistry A. 2003 Nov; 107(44):9380–9386. doi:
862 [10.1021/jp034688o](https://doi.org/10.1021/jp034688o).
- 863 [31] **Eckert F**, Klamt A. Accurate Prediction of Basicity in Aqueous Solution with COSMO-RS. Journal of Computational Chemistry. 2006 Jan;
864 27(1):11–19. doi: [10.1002/jcc.20309](https://doi.org/10.1002/jcc.20309).

- 865 [32] Pracht P, Wilcken R, Udvarhelyi A, Rodde S, Grimme S. High Accuracy Quantum-Chemistry-Based Calculation and Blind Prediction of
866 Macroscopic pKa Values in the Context of the SAMPL6 Challenge. Journal of Computer-Aided Molecular Design. 2018 Oct; 32(10):1139–
867 1149. doi: [10.1007/s10822-018-0145-7](https://doi.org/10.1007/s10822-018-0145-7).
- 868 [33] Prasad S, Huang J, Zeng Q, Brooks BR. An Explicit-Solvent Hybrid QM and MM Approach for Predicting pKa of Small Molecules in SAMPL6
869 Challenge. Journal of Computer-Aided Molecular Design. 2018 Oct; 32(10):1191–1201. doi: [10.1007/s10822-018-0167-1](https://doi.org/10.1007/s10822-018-0167-1).
- 870 [34] Robert Fraczkiewicz MW, SAMPL6 pKa Challenge: Predictions of ionization constants performed by the S+pKa method implemented in
871 ADMET Predictor software; February 22, 2018. The Joint D3R/SAMPL Workshop 2018. <https://drugdesigndata.org/about/d3r-2018-workshop>.
- 872 [35] OEMolProp Toolkit 2017.Feb.1;. OpenEye Scientific Software, Santa Fe, NM. <http://www.eyesopen.com>.

Table S1. SMILES and InChI identifiers of SAMPL6 pK_a Challenge molecules. A CSV version of this table can be found in *SAMPL6-supplementary-documents.tar.gz*.

SAMPL6 Molecule ID	Isomeric SMILES	InChI
SM01	c1cc2c(cc1O)c3c(o2)C(=O)NCCC3	InChI=1S/C12H11NO3/c14-7-3-4-10-9(6-7)8-2-1-5-13-12(15)11(8)16-10/h3-4,6,14H,1-2,5H2,(H,13,15)
SM02	c1ccc2c(c1)c(ncn2)Nc3cccc(c3)C(F)(F)	InChI=1S/C15H10F3N3/c16-15(17,18)10-4-3-5-11(8-10)21-14-12-6-1-2-7-13(12)19-9-20-14/h1-9H,(H,19,20,21)
SM03	c1ccc(cc1)Cc2nnnc(s2)NC(=O)c3cccs3	InChI=1S/C14H11N3OS2/c18-13(11-7-4-8-19-11)15-14-17-16-12(20-14)9-10-5-2-1-3-6-10/h1-8H,9H2,(H,15,17,18)
SM04	c1ccc2c(c1)c(ncn2)NCc3ccc(cc3)Cl	InChI=1S/C15H12ClN3/c16-12-7-5-11(6-8-12)9-17-15-13-3-1-2-4-14(13)18-10-19-15/h1-8,10H,9H2,(H,17,18,19)
SM05	c1ccc(c(c1)NC(=O)c2ccc(o2)Cl)N3CCCCC3	InChI=1S/C16H17ClN2O2/c17-15-9-8-14(21-15)16(20)18-12-6-2-3-7-13(12)19-10-4-1-5-11-19/h2-3,6-9H,1,4-5,10-11H2,(H,18,20)
SM06	c1cc2ccnc2c(c1)NC(=O)c3cc(cnc3)Br	InChI=1S/C15H10BrN3O/c16-12-7-11(8-17-9-12)15(20)19-13-5-1-3-10-4-2-6-18-14(10)13/h1-9H,(H,19,20)
SM07	c1ccc(cc1)CNc2c3cccc3ncn2	InChI=1S/C15H13N3/c1-2-6-12(7-3-1)10-16-15-13-8-4-5-9-14(13)17-11-18-15/h1-9,11H,10H2,(H,16,17,18)
SM08	Cc1ccc2c(c1)c(c(c(=O)[nH]2)CC(=O)O)c3cccc3	InChI=1S/C18H15NO3/c1-11-7-8-15-13(9-11)17(12-5-3-2-4-6-12)14(10-16(20)21)18(22)19-15/h2-9H,10H2,1H3,(H,19,22)(H,20,21)
SM09	COc1cccc(c1)Nc2c3cccc3ncn2.Cl	InChI=1S/C15H13N3O.CIH/c1-19-12-6-4-5-11(9-12)18-15-13-7-2-3-8-14(13)16-10-17-15;/h2-10H,1H3,(H,16,17,18);1H
SM10	c1ccc(cc1)C(=O)NCC(=O)Nc2nc3cccc3s2	InChI=1S/C16H13N3O2S/c20-14(10-17-15(21)11-6-2-1-3-7-11)19-16-18-1-2-8-4-5-9-13(12)22-16/h1-9H,10H2,(H,17,21)(H,18,19,20)
SM11	c1ccc(cc1)n2c3c(cn2)c(ncn3)N	InChI=1S/C11H9N5/c12-10-9-6-15-16(11(9)14-7-13-10)8-4-2-1-3-5-8/h1-7H,(H,2,12,13,14)
SM12	c1ccc2c(c1)c(ncn2)Nc3cccc(c3)Cl.Cl	InChI=1S/C14H10ClN3.CIH/c15-10-4-3-5-11(8-10)18-14-12-6-1-2-7-13(12)16-9-17-14;/h1-9H,(H,16,17,18);1H
SM13	Cc1cccc(c1)Nc2c3cc(c(c3ncn2)OC)OC	InChI=1S/C17H17N3O2/c1-11-5-4-6-12(7-11)20-17-13-8-15(21-2)16(22-3)9-14(13)18-10-19-17/h4-10H,1-3H3,(H,18,19,20)
SM14	c1ccc(cc1)n2ncn3c2ccc(c3)N	InChI=1S/C13H11N3/c14-10-6-7-13-12(8-10)15-9-16(13)11-4-2-1-3-5-11/h1-9H,14H2
SM15	c1ccc2c(c1)ncn2c3ccc(cc3)O	InChI=1S/C13H10N2O/c16-11-7-5-10(6-8-11)15-9-14-12-3-1-2-4-13(12)15/h1-9,16H
SM16	c1cc(c(c(c1)Cl)C(=O)Nc2ccncc2)Cl	InChI=1S/C12H8Cl2N2O/c13-9-2-1-3-10(14)11(9)12(17)16-8-4-6-15-7-5-8/h1-7H,(H,15,16,17)
SM17	c1ccc(cc1)CSc2nnc(o2)c3ccncc3	InChI=1S/C14H11N3OS/c1-2-4-11(5-3-1)10-19-14-17-16-13(18-14)12-6-8-15-9-7-12/h1-9H,10H2
SM18	c1ccc2c(c1)c(=O)[nH]c(n2)CCC(=O)Nc3ncc(s3)Cc4ccc(c(c4)F)F	InChI=1S/C21H16F2N4O2S/c22-15-6-5-12(10-16(15)23)9-13-11-24-21(30-13)27-19(28)8-7-18-25-17-4-2-1-3-14(17)20(29)26-18/h1-6,10-11H,7-9H2,(H,24,27,28)(H,25,26,29)
SM19	CCOc1ccc2c(c1)sc(n2)NC(=O)Cc3ccc(c(c3)Cl)Cl	InChI=1S/C17H14Cl2N2O2S/c1-2-23-11-4-6-14-15(9-11)24-17(20-14)21-6(22)8-10-3-5-12(18)13(9)7-10/h3-7,9H,2,8H2,1H3,(H,20,21,22)
SM20	c1cc(cc(c1)OCc2ccc(cc2Cl)Cl)/C=C/3\C(=O)NC(=O)S3	InChI=1S/C17H11Cl2NO3S/c18-12-5-4-11(14(19)8-12)9-23-13-3-1-2-10(6-13)7-15-16(21)20-17(22)24-15/h1-8H,9H2,(H,20,21,22)/b15-7+
SM21	c1cc(cc(c1)Br)Nc2c(cnc(n2)Nc3cccc(c3)Br)F	InChI=1S/C16H11Br2FN4/c17-10-3-1-5-12(7-10)21-15-14(19)9-20-16(23-15)22-13-6-2-4-11(18)8-13/h1-9H,(H,20,21,22,23)
SM22	c1cc2c(cc(c(c2nc1)O))l	InChI=1S/C9H5l2NO/c10-6-4-7(11)9(13)8-5(6)2-1-3-12-8/h1-4,13H
SM23	CCOC(=O)c1ccc(cc1)Nc2cc(cnc(n2)Nc3ccc(cc3)C(=O)OCC)C	InChI=1S/C23H24N4O4/c1-4-30-21(28)16-6-10-18(11-7-16)25-20-14-15(3)24-23(27-20)26-19-12-8-17(9-13-19)22(29)31-5-2/h6-14H,4-5H2,1-3H3,(H2,24,25,26,27)
SM24	COc1ccc(cc1)c2c3c(ncn3oc2c4ccc(cc4)OC)NCCO	InChI=1S/C22H21N3O4/c1-27-16-7-3-14(4-8-16)18-19-21(23-11-12-26)24-13-25-22(19)29-20(18)15-5-9-17(28-2)10-6-15/h3-10,13,26H,11-12H2,1-2H3,(H,23,24,25)

10 Supplementary Information

Table S2. Evaluation statistics calculated for all macroscopic pK_a prediction submissions based on Hungarian match for 24 molecules. Methods are represented via their SAMPL6 submission IDs which can be cross referenced with Table 1 for method details. There are eight error metrics reported: the root-mean-squared error (RMSE), mean absolute error (MAE), mean (signed) error (ME), coefficient of determination (R^2), linear regression slope (m), Kendall's Rank Correlation Coefficient (τ), unmatched experimental pK_as (number of missing pK_a predictions) and unmatched predicted pK_as (number of extra pK_a predictions between 2 and 12. This table is ranked by increasing RMSE. A CSV version of this table can be found in *SAMPL6-supplementary-documents.tar.gz*.

Submission ID	RMSE	MAE	ME	R ²	m	Kendall's Tau	Unmatched exp. pK _a s	Unmatched pred. pK _a s [2,12]
<i>vxxzd</i>	0.68 [0.54, 0.81]	0.58 [0.45, 0.71]	0.24 [-0.01, 0.45]	0.94 [0.88, 0.97]	0.92 [0.84, 1.02]	0.82 [0.68, 0.92]	2	4
<i>gyuhx</i>	0.73 [0.55, 0.91]	0.59 [0.44, 0.74]	0.03 [-0.23, 0.28]	0.93 [0.88, 0.96]	0.98 [0.90, 1.08]	0.88 [0.80, 0.94]	0	7
<i>xmyhm</i>	0.79 [0.52, 1.03]	0.56 [0.38, 0.77]	0.13 [-0.14, 0.41]	0.92 [0.85, 0.97]	0.96 [0.86, 1.08]	0.81 [0.68, 0.90]	0	3
<i>nb017</i>	0.94 [0.72, 1.16]	0.77 [0.58, 0.97]	-0.16 [-0.49, 0.16]	0.88 [0.81, 0.94]	0.94 [0.82, 1.08]	0.73 [0.60, 0.84]	0	6
<i>nb007</i>	0.95 [0.73, 1.15]	0.78 [0.60, 0.97]	0.05 [-0.29, 0.37]	0.88 [0.77, 0.95]	0.84 [0.77, 0.92]	0.79 [0.65, 0.89]	0	13
<i>yqkga</i>	1.01 [0.78, 1.23]	0.80 [0.59, 1.03]	-0.17 [-0.51, 0.19]	0.87 [0.78, 0.93]	0.93 [0.77, 1.08]	0.83 [0.72, 0.91]	0	1
<i>nb010</i>	1.03 [0.77, 1.26]	0.81 [0.61, 1.04]	0.24 [-0.11, 0.59]	0.87 [0.77, 0.94]	0.95 [0.83, 1.08]	0.80 [0.67, 0.90]	0	4
<i>8xt50</i>	1.07 [0.78, 1.36]	0.81 [0.58, 1.07]	-0.47 [-0.82, -0.14]	0.91 [0.84, 0.95]	1.08 [0.94, 1.22]	0.80 [0.68, 0.89]	0	0
<i>nb013</i>	1.10 [0.72, 1.47]	0.80 [0.56, 1.09]	-0.15 [-0.55, 0.22]	0.88 [0.78, 0.95]	1.09 [0.90, 1.25]	0.79 [0.64, 0.90]	0	6
<i>nb015</i>	1.27 [0.98, 1.56]	1.04 [0.80, 1.31]	0.13 [-0.32, 0.56]	0.87 [0.80, 0.93]	1.16 [0.94, 1.34]	0.78 [0.66, 0.86]	0	0
<i>p0jba</i>	1.31 [0.69, 1.73]	1.08 [0.43, 1.72]	-0.92 [-1.72, -0.11]	0.91 [0.51, 1.00]	1.18 [0.36, 1.72]	0.80 [0.00, 1.00]	0	0
<i>37xrn8</i>	1.41 [0.93, 1.84]	1.01 [0.68, 1.38]	-0.18 [-0.69, 0.32]	0.83 [0.70, 0.93]	1.16 [0.98, 1.33]	0.70 [0.56, 0.83]	1	1
<i>mkhqa</i>	1.60 [1.13, 2.05]	1.24 [0.90, 1.62]	-0.32 [-0.89, 0.21]	0.80 [0.67, 0.91]	1.14 [0.98, 1.34]	0.64 [0.44, 0.79]	0	6
<i>ttjd0</i>	1.64 [1.20, 2.06]	1.30 [0.96, 1.67]	-0.12 [-0.70, 0.45]	0.81 [0.69, 0.91]	1.2 [1.03, 1.40]	0.65 [0.47, 0.80]	0	5
<i>nb001</i>	1.68 [1.05, 2.37]	1.21 [0.84, 1.68]	0.44 [-0.10, 1.03]	0.80 [0.70, 0.90]	1.16 [0.95, 1.42]	0.72 [0.55, 0.85]	0	7
<i>nb002</i>	1.70 [1.08, 2.38]	1.25 [0.89, 1.70]	0.51 [-0.04, 1.10]	0.80 [0.70, 0.90]	1.15 [0.95, 1.42]	0.72 [0.56, 0.84]	0	7
<i>35bdm</i>	1.72 [0.66, 2.34]	1.44 [0.62, 2.26]	-1.01 [-2.18, 0.13]	0.92 [0.46, 1.00]	1.45 [0.73, 2.15]	0.80 [0.00, 1.00]	0	0
<i>ryzue</i>	1.77 [1.42, 2.12]	1.50 [1.17, 1.84]	1.30 [0.86, 1.72]	0.91 [0.86, 0.95]	1.23 [1.06, 1.41]	0.82 [0.71, 0.91]	0	0
<i>2ii2g</i>	1.80 [1.31, 2.24]	1.39 [1.01, 1.82]	-0.74 [-1.29, -0.15]	0.79 [0.65, 0.89]	1.15 [0.96, 1.37]	0.68 [0.59, 0.82]	0	2
<i>mpwiy</i>	1.82 [1.39, 2.23]	1.48 [1.14, 1.88]	0.10 [-0.54, 0.73]	0.82 [0.70, 0.91]	1.29 [1.12, 1.51]	0.66 [0.49, 0.80]	0	5
<i>5byn6</i>	1.89 [1.50, 2.27]	1.59 [1.24, 1.97]	1.32 [0.84, 1.80]	0.91 [0.85, 0.95]	1.28 [1.10, 1.48]	0.83 [0.72, 0.92]	0	0
<i>y75vj</i>	1.90 [1.50, 2.26]	1.58 [1.21, 1.97]	1.04 [0.46, 1.60]	0.89 [0.79, 0.95]	1.34 [1.16, 1.53]	0.75 [0.57, 0.88]	1	0
<i>w4iyd</i>	1.93 [1.53, 2.28]	1.58 [1.20, 1.98]	1.26 [0.72, 1.76]	0.85 [0.74, 0.92]	1.21 [1.00, 1.40]	0.73 [0.57, 0.85]	0	1
<i>np6b4</i>	1.94 [1.21, 2.71]	1.44 [1.04, 1.94]	-0.47 [-1.08, 0.24]	0.71 [0.60, 0.87]	1.08 [0.81, 1.43]	0.75 [0.62, 0.86]	0	8
<i>nb004</i>	2.01 [1.38, 2.63]	1.57 [1.16, 2.04]	0.56 [-0.10, 1.27]	0.82 [0.72, 0.90]	1.35 [1.15, 1.60]	0.71 [0.54, 0.84]	0	5
<i>nb003</i>	2.01 [1.39, 2.64]	1.58 [1.18, 2.04]	0.52 [-0.14, 1.22]	0.82 [0.73, 0.91]	1.36 [1.16, 1.61]	0.71 [0.54, 0.84]	0	5
<i>yc70m</i>	2.03 [1.73, 2.33]	1.80 [1.48, 2.13]	-0.41 [-1.09, 0.31]	0.47 [0.28, 0.64]	0.56 [0.35, 0.83]	0.53 [0.35, 0.68]	0	27
<i>hytjn</i>	2.16 [1.24, 3.06]	1.39 [0.86, 2.04]	0.71 [0.03, 1.48]	0.45 [0.13, 0.78]	0.62 [0.26, 1.00]	0.47 [0.16, 0.73]	1	27
<i>f0gew</i>	2.18 [1.38, 2.95]	1.58 [1.09, 2.16]	-0.73 [-1.42, 0.04]	0.77 [0.67, 0.89]	1.29 [1.01, 1.63]	0.76 [0.63, 0.86]	0	0
<i>q3pfp</i>	2.19 [1.33, 3.09]	1.51 [0.99, 2.13]	0.59 [-0.10, 1.37]	0.44 [0.13, 0.77]	0.66 [0.27, 1.07]	0.50 [0.20, 0.75]	1	22
<i>ds62k</i>	2.22 [1.62, 2.81]	1.78 [1.34, 2.27]	0.78 [0.06, 1.52]	0.82 [0.70, 0.90]	1.41 [1.20, 1.63]	0.72 [0.55, 0.85]	0	4
<i>xikp8</i>	2.35 [1.94, 2.73]	2.06 [1.66, 2.47]	0.77 [-0.02, 1.58]	0.89 [0.80, 0.95]	1.59 [1.40, 1.81]	0.76 [0.59, 0.89]	1	0
<i>nb005</i>	2.38 [1.79, 2.95]	1.91 [1.44, 2.43]	0.31 [-0.49, 1.15]	0.84 [0.74, 0.91]	1.56 [1.34, 1.82]	0.71 [0.54, 0.83]	0	0
<i>5nm4j</i>	2.45 [1.42, 3.34]	1.58 [0.94, 2.34]	0.05 [-0.80, 1.07]	0.19 [0.00, 0.70]	0.40 [-0.06, 0.81]	0.34 [-0.04, 0.67]	4	1
<i>ad5pu</i>	2.54 [1.68, 3.30]	1.83 [1.24, 2.49]	-0.65 [-1.48, 0.25]	0.76 [0.64, 0.88]	1.43 [1.12, 1.78]	0.77 [0.63, 0.88]	0	0
<i>pwn3m</i>	2.60 [1.45, 3.53]	1.54 [0.83, 2.37]	0.79 [-0.06, 1.77]	0.21 [0.00, 0.63]	0.37 [0.01, 0.78]	0.34 [0.04, 0.63]	1	3
<i>nb006</i>	2.98 [2.37, 3.56]	2.53 [2.00, 3.10]	0.42 [-0.60, 1.47]	0.84 [0.74, 0.92]	1.78 [1.55, 2.06]	0.71 [0.54, 0.84]	0	0
<i>0hxtm</i>	3.26 [1.81, 4.39]	1.92 [1.03, 2.98]	1.38 [0.37, 2.56]	0.08 [0.00, 0.48]	0.28 [-0.17, 0.83]	0.29 [-0.04, 0.61]	3	7

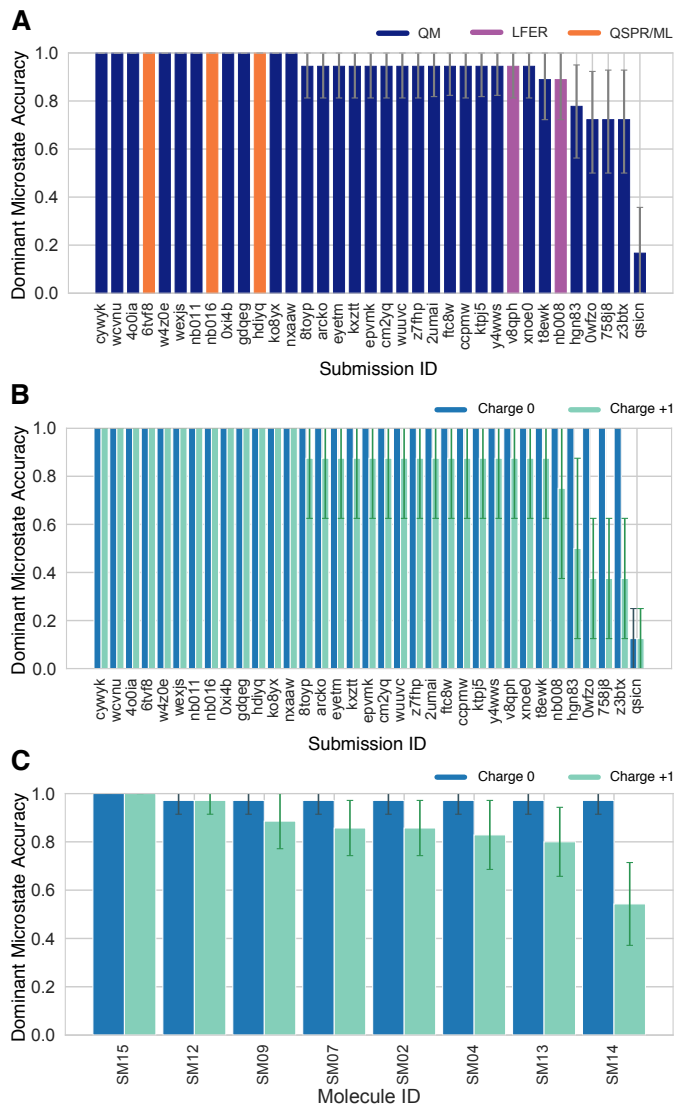
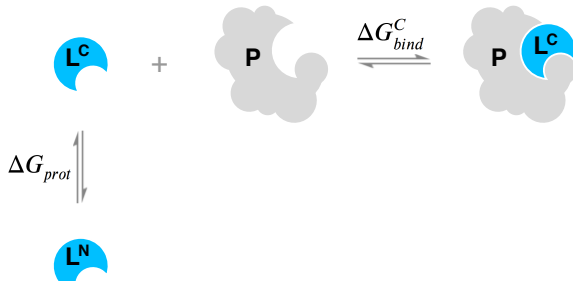


Figure 10. Some methods predicted the sequence of dominant tautomers inaccurately. Prediction accuracy of dominant microstate of each charged state was calculated using the dominant microstate sequence determined by NMR for 8 molecules as reference. **(A)** Dominant microstate accuracy vs. submission ID plot was calculated considering all the dominant microstates seen in the 8 molecule experimental microstate dataset. **(B)** Dominant microstate accuracy vs. submission ID plot was generated considering only the dominant microstates of charge 0 and +1 seen in the 8 molecule experimental microstate dataset. Accuracy of each molecule is broken out by total charge of the microstate. **(C)** Dominant microstate prediction accuracy calculated for each molecule averaged over all methods. In **(B)** and **(C)**, the accuracy of predicting the dominant neutral tautomer is showed in blue and the accuracy of predicting the dominant +1 charged tautomer is showed in green. Error bars denoting 95% confidence intervals obtained by bootstrapping.

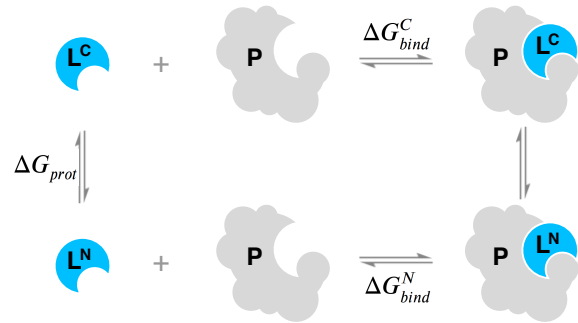
A When only the minor protonation state can bind to the protein



$$\Delta G_{bind} = \Delta G_{bind}^C + \Delta G_{prot}$$

$$\Delta G_{bind} = \Delta G_{bind}^C + RT(pH - pK_a) \ln(10)$$

B When multiple protonation states can bind to the protein



$$\Delta G_{bind} = \Delta G_{bind}^N + \Delta G_{corr}$$

$$\Delta G_{bind} = \Delta G_{bind}^N - RT \ln \frac{1 + e^{-\frac{\Delta G_{bind}^C - \Delta G_{bind}^N}{RT}} 10^{pK_a - pH}}{1 + 10^{pK_a - pH}}$$

Figure 11. Aqueous pK_a of the ligand can influence overall protein-ligand binding affinity. **A** When only the minor aqueous protonation state contributes to protein-ligand complex formation, overall binding free energy (ΔG_{bind}) needs to be calculated as the sum of binding affinity of the minor state and the protonation penalty of that state. **B** When multiple charge states contribute to complex formation, overall free energy of binding includes a multiple protonation states correction (MPSC) term (ΔG_{corr}). MPSC is a function of pH, aqueous pK_a of the ligand, and the difference between the binding free energy of charged and neutral species ($\Delta G_{bind}^C - \Delta G_{bind}^N$).

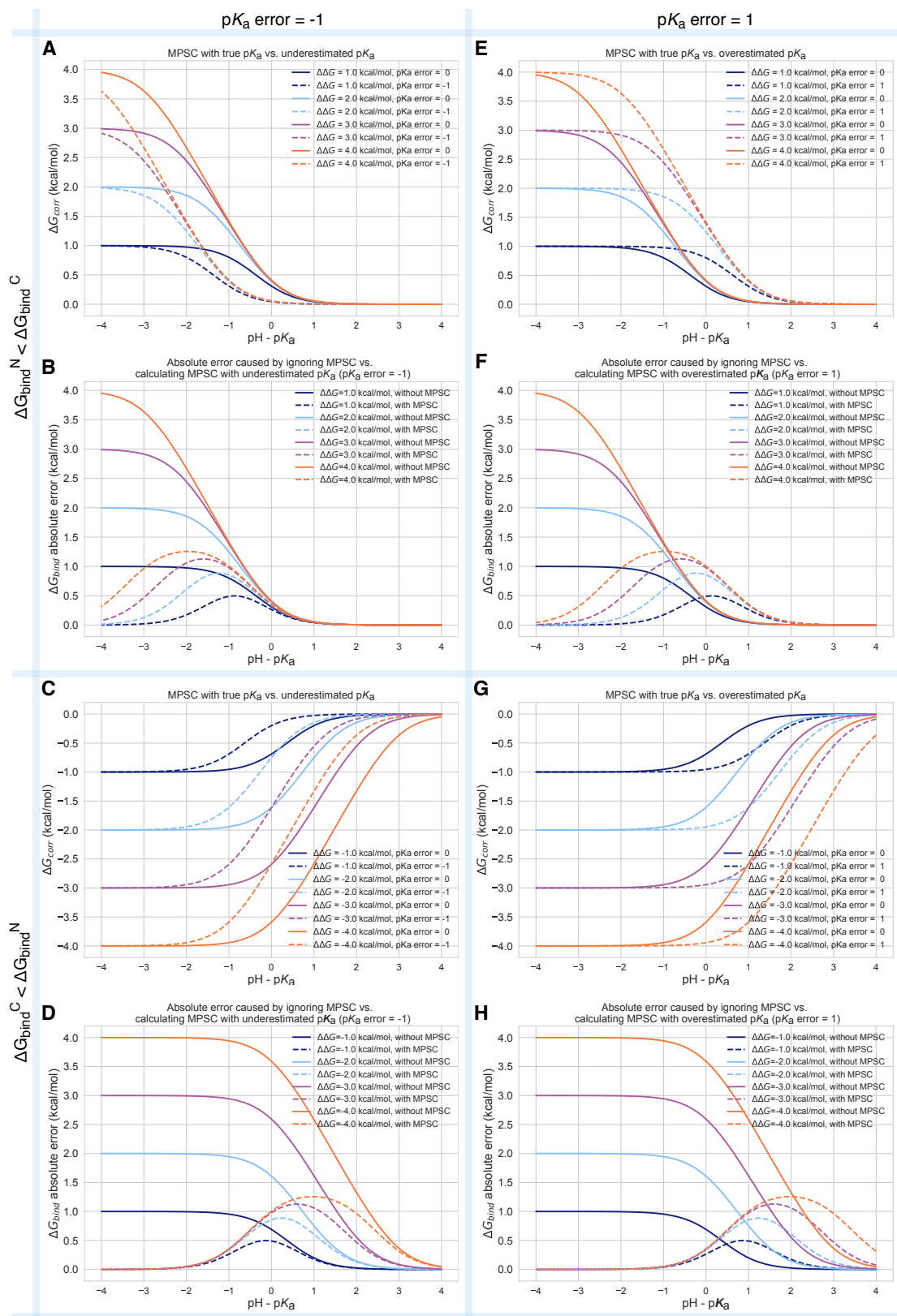


Figure 12. Inaccuracy of pK_a prediction (± 1 unit) affects the accuracy of MPSC and overall protein-ligand binding free energy calculation in varying amounts based on aqueous pK_a value and relative binding affinity of individual protonation states ($\Delta\Delta G = \Delta G_{bind}^C - \Delta G_{bind}^N$). All calculations are made for 25°C, and for a ligand with single basic titratable group. **A, C, E, and G show MPSC (ΔG_{corr}) calculated with true vs. inaccurate pK_a . **B, D, F, and H** show comparison of the absolute error to ΔG_{bind} caused by ignoring the MPSC completely (solid lines) vs. calculating MPSC based in inaccurate pK_a value (dashed lines). These plots provide guidance on when it is beneficial to include MPSC correction based on pK_a error, $pH - pK_a$, and $\Delta\Delta G$.**

Table S3. Evaluation statistics calculated for all microscopic pK_a prediction submissions based on Hungarian match for 8 molecules with NMR data. Methods are represented via their SAMPL6 submission IDs which can be cross referenced with Table 1 for method details. There are eight error metrics reported: the root-mean-squared error (RMSE), mean absolute error (MAE), mean (signed) error (ME), coefficient of determination (R^2), linear regression slope (m), Kendall's Rank Correlation Coefficient (τ), unmatched experimental pK_as (number of missing pK_a predictions) and unmatched predicted pK_as (number of extra pK_a predictions between 2 and 12. This table is ranked by increasing RMSE. A CSV version of this table can be found in *SAMPL6-supplementary-documents.tar.gz*.

Submission ID	RMSE	MAE	ME	R ²	m	Kendall's Tau	Unmatched exp. pK _a s	Unmatched pred. pK _a s [2,12]
<i>nb011</i>	0.47 [0.30, 0.64]	0.33 [0.22, 0.46]	-0.02 [-0.18, 0.14]	0.97 [0.94, 0.99]	1.01 [0.97, 1.06]	0.90 [0.78, 0.96]	0	36
<i>hdlyq</i>	0.62 [0.47, 0.76]	0.47 [0.33, 0.62]	0.13 [-0.09, 0.34]	0.95 [0.92, 0.97]	0.34 [0.92, 1.09]	0.87 [0.79, 0.93]	0	16
<i>epvmk</i>	0.63 [0.43, 0.81]	0.47 [0.32, 0.63]	-0.02 [-0.25, 0.21]	0.95 [0.89, 0.98]	0.21 [0.91, 1.04]	0.81 [0.68, 0.91]	0	37
<i>xnoe0</i>	0.65 [0.47, 0.82]	0.50 [0.36, 0.66]	-0.1 [-0.32, 0.13]	0.95 [0.89, 0.98]	0.13 [0.92, 1.05]	0.82 [0.69, 0.91]	0	36
<i>gdqeg</i>	0.65 [0.41, 0.89]	0.43 [0.27, 0.62]	0.11 [-0.10, 0.35]	0.94 [0.88, 0.98]	0.35 [0.87, 1.02]	0.83 [0.67, 0.95]	0	53
<i>4o0ia</i>	0.66 [0.44, 0.86]	0.47 [0.31, 0.64]	0.00 [-0.22, 0.24]	0.94 [0.88, 0.98]	0.24 [0.87, 1.05]	0.85 [0.73, 0.94]	0	35
<i>nb008</i>	0.76 [0.48, 1.02]	0.52 [0.34, 0.73]	-0.08 [-0.37, 0.17]	0.93 [0.85, 0.98]	0.17 [0.79, 0.93]	0.84 [0.73, 0.92]	0	35
<i>ccpmw</i>	0.79 [0.62, 0.94]	0.62 [0.46, 0.80]	-0.17 [-0.44, 0.11]	0.92 [0.86, 0.96]	0.11 [0.82, 1.05]	0.80 [0.67, 0.89]	0	7
<i>0xi4b</i>	0.84 [0.58, 1.07]	0.61 [0.42, 0.83]	0.22 [-0.07, 0.51]	0.92 [0.84, 0.97]	0.51 [0.91, 1.09]	0.81 [0.65, 0.92]	0	32
<i>cwyk</i>	0.86 [0.60, 1.10]	0.62 [0.42, 0.84]	0.13 [-0.16, 0.44]	0.90 [0.82, 0.96]	0.44 [0.86, 1.08]	0.81 [0.64, 0.92]	0	35
<i>ftc8w</i>	0.86 [0.51, 1.17]	0.59 [0.39, 0.83]	0.10 [-0.19, 0.41]	0.90 [0.77, 0.97]	0.41 [0.84, 0.98]	0.75 [0.57, 0.88]	0	35
<i>nxaaw</i>	0.89 [0.56, 1.25]	0.61 [0.41, 0.87]	-0.02 [-0.35, 0.28]	0.89 [0.75, 0.97]	0.28 [0.85, 1.00]	0.79 [0.63, 0.91]	0	29
<i>nb016</i>	0.95 [0.71, 1.18]	0.77 [0.57, 0.98]	-0.23 [-0.56, 0.12]	0.89 [0.83, 0.95]	0.12 [0.82, 1.07]	0.75 [0.62, 0.85]	0	3
<i>kxzt</i>	0.96 [0.56, 1.33]	0.64 [0.41, 0.92]	0.00 [-0.32, 0.36]	0.90 [0.76, 0.97]	0.36 [0.96, 1.13]	0.79 [0.63, 0.91]	0	37
<i>eyetm</i>	0.98 [0.69, 1.27]	0.72 [0.50, 0.97]	-0.32 [-0.65, 0.00]	0.91 [0.86, 0.96]	0.00 [0.94, 1.22]	0.78 [0.64, 0.88]	0	7
<i>cm2yq</i>	0.99 [0.44, 1.54]	0.56 [0.31, 0.90]	0.10 [-0.21, 0.50]	0.91 [0.83, 0.98]	0.50 [0.96, 1.25]	0.89 [0.80, 0.96]	0	36
<i>2umai</i>	1.00 [0.46, 1.54]	0.57 [0.33, 0.91]	0.07 [-0.25, 0.46]	0.91 [0.82, 0.98]	0.46 [0.96, 1.26]	0.87 [0.76, 0.95]	0	36
<i>ko8yx</i>	1.01 [0.76, 1.25]	0.78 [0.56, 1.01]	0.35 [0.01, 0.67]	0.91 [0.82, 0.96]	0.67 [0.96, 1.19]	0.78 [0.64, 0.89]	0	26
<i>wuuvc</i>	1.02 [0.51, 1.53]	0.62 [0.38, 0.93]	0.19 [-0.13, 0.58]	0.88 [0.80, 0.96]	0.58 [0.85, 1.19]	0.90 [0.81, 0.96]	0	36
<i>ktpj5</i>	1.02 [0.51, 1.56]	0.61 [0.37, 0.95]	0.17 [-0.16, 0.57]	0.88 [0.80, 0.96]	0.57 [0.87, 1.22]	0.89 [0.80, 0.96]	0	36
<i>z7fhp</i>	1.02 [0.49, 1.55]	0.61 [0.36, 0.94]	0.08 [-0.24, 0.48]	0.90 [0.82, 0.97]	0.48 [0.97, 1.26]	0.88 [0.80, 0.95]	0	28
<i>arcko</i>	1.04 [0.73, 1.32]	0.77 [0.53, 1.02]	0.37 [0.05, 0.72]	0.89 [0.80, 0.94]	0.72 [0.90, 1.14]	0.78 [0.62, 0.90]	0	24
<i>y4wws</i>	1.04 [0.70, 1.33]	0.74 [0.49, 1.00]	-0.31 [-0.66, 0.05]	0.91 [0.85, 0.96]	0.05 [1.02, 1.26]	0.79 [0.68, 0.88]	0	30
<i>wcvnu</i>	1.11 [0.80, 1.39]	0.84 [0.59, 1.11]	0.28 [-0.10, 0.66]	0.89 [0.77, 0.95]	0.66 [0.98, 1.22]	0.73 [0.54, 0.88]	1	27
<i>8toyp</i>	1.13 [0.61, 1.65]	0.70 [0.42, 1.05]	0.13 [-0.25, 0.56]	0.88 [0.81, 0.96]	0.56 [0.98, 1.29]	0.83 [0.72, 0.92]	0	27
<i>qsicn</i>	1.17 [0.30, 1.65]	0.88 [0.23, 1.54]	-0.76 [-1.54, 0.01]	0.91 [0.46, 1.00]	0.01 [0.52, 1.59]	0.80 [0.00, 1.00]	0	2
<i>wexjs</i>	1.30 [0.95, 1.62]	0.98 [0.68, 1.29]	0.27 [-0.17, 0.74]	0.86 [0.74, 0.93]	0.74 [1.00, 1.29]	0.73 [0.55, 0.86]	0	25
<i>v8qph</i>	1.37 [0.92, 1.79]	0.98 [0.66, 1.34]	-0.15 [-0.64, 0.34]	0.84 [0.70, 0.93]	0.34 [0.97, 1.32]	0.70 [0.55, 0.82]	0	6
<i>w420e</i>	1.57 [1.18, 1.94]	1.23 [0.90, 1.58]	0.09 [-0.48, 0.62]	0.85 [0.76, 0.91]	0.62 [1.08, 1.46]	0.72 [0.60, 0.82]	0	19
<i>6tvf8</i>	1.88 [0.87, 2.85]	1.02 [0.54, 1.66]	0.45 [-0.14, 1.18]	0.51 [0.16, 0.87]	1.18 [0.26, 0.89]	0.61 [0.34, 0.82]	0	55
<i>0wfzo</i>	2.89 [1.73, 3.89]	1.88 [1.17, 2.68]	0.76 [-0.15, 1.77]	0.48 [0.21, 0.75]	1.77 [0.60, 1.37]	0.51 [0.30, 0.70]	0	4
<i>t8ewk</i>	3.30 [1.89, 4.39]	1.98 [1.06, 3.00]	1.32 [0.27, 2.49]	0.07 [0.00, 0.45]	2.49 [-0.17, 0.79]	0.28 [-0.03, 0.6]	0	6
<i>z3btx</i>	4.00 [2.30, 5.45]	2.49 [1.47, 3.65]	1.48 [0.26, 2.86]	0.29 [0.04, 0.60]	2.86 [0.31, 1.44]	0.43 [0.19, 0.63]	0	1
<i>758j8</i>	4.52 [2.64, 6.18]	2.95 [1.85, 4.25]	1.85 [0.48, 3.38]	0.24 [0.02, 0.58]	3.38 [0.20, 1.51]	0.34 [0.08, 0.57]	0	2
<i>hgn83</i>	6.38 [4.04, 8.47]	4.11 [2.52, 5.93]	2.13 [0.07, 4.28]	0.08 [0.00, 0.39]	4.28 [-0.18, 1.43]	0.32 [0.07, 0.56]	0	0

Table S4. Evaluation statistics calculated for all microscopic pK_a prediction submissions based on microstate pair match for 8 molecules with NMR data. Methods are represented via their SAMPL6 submission IDs which can be cross referenced with Table 1 for method details. There are eight error metrics reported: the root-mean-squared error (RMSE), mean absolute error (MAE), mean (signed) error (ME), coefficient of determination (R^2), linear regression slope (m), Kendall's Rank Correlation Coefficient (τ), unmatched experimental pK_as (number of missing pK_a predictions) and unmatched predicted pK_as (number of extra pK_a predictions between 2 and 12. This table is ranked by increasing RMSE. A CSV version of this table can be found in *SAMPL6-supplementary-documents.tar.gz*.

Update this table with dominant microstate accuracy

Submission ID	RMSE	MAE	ME	R^2	m	Kendall's Tau	Unmatched exp. pK _a s	Unmatched pred. pK _a s [2,12]
nb016	0.52 [0.25, 0.71]	0.43 [0.23, 0.65]	-0.09 [-0.45, 0.30]	0.92 [0.05, 0.99]	0.99 [0.14, 1.16]	0.62 [-0.14, 1.00]	0	3
hdlyq	0.68 [0.49, 0.83]	0.60 [0.39, 0.80]	0.38 [0.02, 0.70]	0.86 [0.47, 0.98]	0.91 [0.45, 1.26]	0.78 [0.4, 1.00]	0	16
nb011	0.72 [0.35, 1.07]	0.54 [0.28, 0.86]	0.45 [0.14, 0.83]	0.86 [0.18, 0.98]	0.93 [0.50, 1.21]	0.64 [0.26, 0.95]	0	36
ftc8w	0.75 [0.52, 0.96]	0.68 [0.50, 0.89]	-0.31 [-0.68, 0.16]	0.87 [0.02, 0.99]	1.12 [-0.11, 1.39]	0.56 [-0.10, 1.00]	0	35
6tvf8	0.76 [0.55, 0.95]	0.68 [0.46, 0.90]	-0.63 [-0.89, -0.35]	0.92 [0.78, 0.99]	0.94 [0.69, 1.41]	0.87 [0.6, 1.00]	0	55
t8ewk	0.96 [0.65, 1.19]	0.81 [0.46, 1.13]	-0.77 [-1.12, -0.38]	0.80 [0.53, 0.96]	0.96 [0.76, 2.26]	0.78 [0.31, 1.00]	1	7
v8qph	0.99 [0.40, 1.52]	0.67 [0.29, 1.17]	-0.09 [-0.75, 0.45]	0.68 [0.11, 0.97]	0.96 [-1.26, 1.16]	0.38 [-0.3, 1.00]	0	6
ccpmw	1.07 [0.78, 1.27]	0.95 [0.60, 1.25]	-0.83 [-1.25, -0.37]	0.74 [0.43, 0.99]	0.95 [0.70, 2.32]	0.89 [0.52, 1.00]	1	8
0xi4b	1.15 [0.75, 1.50]	0.98 [0.63, 1.36]	-0.30 [-0.94, 0.44]	0.77 [0.02, 0.98]	1.26 [0.09, 2.10]	0.51 [-0.14, 1.00]	0	33
cywyk	1.17 [0.88, 1.41]	1.06 [0.74, 1.35]	-0.47 [-1.09, 0.24]	0.73 [0.02, 0.98]	1.15 [-0.04, 2.00]	0.56 [-0.08, 1.00]	0	36
eyetm	1.17 [0.77, 1.52]	1.00 [0.61, 1.41]	-0.89 [-1.38, -0.38]	0.67 [0.30, 0.94]	0.93 [0.65, 2.59]	0.72 [0.29, 1.00]	1	8
nb008	1.26 [0.74, 1.71]	1.09 [0.63, 1.57]	0.47 [-0.40, 1.32]	0.79 [0.01, 0.99]	1.21 [-0.59, 1.85]	0.52 [-0.2, 1.00]	0	38
y4wws	1.41 [0.95, 1.80]	1.22 [0.78, 1.66]	-0.71 [-1.44, 0.06]	0.87 [0.05, 0.98]	1.55 [0.41, 2.02]	0.56 [-0.11, 1.00]	0	31
ktpj5	1.46 [0.83, 2.10]	1.15 [0.67, 1.77]	0.94 [0.29, 1.68]	0.77 [0.01, 0.98]	1.28 [-0.26, 1.60]	0.42 [-0.27, 0.95]	0	37
wuuvc	1.47 [0.84, 2.09]	1.18 [0.70, 1.77]	0.99 [0.36, 1.68]	0.78 [0.01, 0.98]	1.27 [-0.24, 1.58]	0.47 [-0.20, 1.00]	0	37
xnoe0	1.54 [1.09, 2.00]	1.39 [1.02, 1.83]	0.91 [0.11, 1.64]	0.82 [0.01, 0.98]	1.47 [-0.30, 1.79]	0.42 [-0.27, 0.95]	0	37
qsicn	1.58 [1.44, 1.70]	1.57 [1.44, 1.70]	-1.57 [-1.7, -1.44]	1.00 [0.00, 1.00]	1.06		0	2
epvmk	1.66 [1.20, 2.15]	1.50 [1.07, 1.96]	1.12 [0.31, 1.82]	0.82 [0.02, 0.98]	1.47 [-0.21, 1.8]	0.42 [-0.25, 0.95]	0	37
400ia	1.73 [1.33, 2.17]	1.62 [1.29, 2.02]	1.31 [0.53, 1.93]	0.87 [0.03, 0.99]	1.50 [0.07, 1.84]	0.56 [-0.07, 1.00]	0	36
ko8yx	1.75 [1.08, 2.45]	1.44 [0.87, 2.12]	1.38 [0.74, 2.10]	0.97 [0.88, 1.00]	1.66 [1.46, 2.28]	0.91 [0.69, 1.00]	0	27
2umai	1.76 [1.21, 2.35]	1.54 [1.04, 2.11]	1.31 [0.55, 2.03]	0.82 [0.02, 0.98]	1.43 [-0.02, 1.77]	0.47 [-0.17, 0.95]	0	37
cm2yq	1.77 [1.22, 2.36]	1.55 [1.06, 2.12]	1.33 [0.57, 2.04]	0.82 [0.02, 0.98]	1.43 [-0.02, 1.76]	0.47 [-0.17, 0.95]	0	37
nxaaw	1.80 [0.84, 2.80]	1.34 [0.80, 2.18]	0.16 [-0.77, 1.41]	0.59 [0.02, 0.97]	1.37 [-0.08, 2.92]	0.6 [-0.05, 1.00]	0	30
wcvnu	1.90 [1.14, 2.64]	1.57 [0.97, 2.27]	1.44 [0.70, 2.24]	0.97 [0.91, 1.00]	1.78 [1.58, 2.48]	0.91 [0.69, 1.00]	0	27
kxzt	2.00 [1.13, 2.73]	1.64 [1.00, 2.39]	1.64 [1.00, 2.39]	0.83 [0.01, 0.98]	1.42 [-0.21, 1.99]	0.56 [-0.10, 1.00]	0	38
wexjs	2.05 [1.18, 2.93]	1.66 [1.01, 2.47]	1.48 [0.63, 2.39]	0.96 [0.55, 0.99]	1.87 [1.54, 2.29]	0.73 [0.20, 1.00]	0	26
z7fhp	2.14 [1.38, 2.87]	1.80 [1.12, 2.58]	1.28 [0.18, 2.34]	0.78 [0.02, 0.98]	1.71 [-0.41, 2.13]	0.42 [-0.25, 0.95]	0	30
gdqeg	2.38 [1.97, 2.71]	2.25 [1.74, 2.68]	-1.61 [-2.46, -0.37]	0.10 [0.00, 0.98]	0.31 [-0.60, 1.63]	0.29 [-0.45, 1.00]	0	53
8toyp	2.63 [1.89, 3.29]	2.34 [1.59, 3.07]	1.78 [0.47, 2.89]	0.82 [0.02, 0.98]	1.94 [-0.06, 2.39]	0.47 [-0.17, 0.95]	0	29
w420e	2.63 [1.81, 3.53]	2.34 [1.67, 3.18]	1.74 [0.46, 2.92]	0.98 [0.55, 1.00]	2.28 [1.52, 2.41]	0.73 [0.20, 1.00]	0	20
arcko	2.64 [1.23, 3.78]	2.08 [1.10, 3.24]	1.71 [0.44, 3.10]	0.57 [0.04, 0.95]	1.42 [0.56, 2.93]	0.56 [-0.06, 1.00]	0	28
0wfzo	18.72 [11.21, 25.03]	15.80 [9.9, 22.35]	15.09 [8.28, 22.12]	0.09 [0.01, 0.73]	2.35 [-10.18, 8.12]	0.02 [-0.65, 0.66]	0	12
z3btv	22.60 [15.03, 29.00]	19.70 [12.97, 26.69]	19.70 [12.97, 26.69]	0.09 [0.01, 0.72]	2.35 [-10.00, 8.28]	0.02 [-0.66, 0.66]	0	7
758j8	23.76 [16.33, 30.24]	21.00 [14.26, 28.00]	21.00 [14.26, 28.00]	0.09 [0.01, 0.71]	2.35 [-10.34, 8.12]	0.02 [-0.65, 0.65]	0	8
hgn83	27.91 [20.54, 34.52]	25.60 [18.9, 32.64]	25.60 [18.9, 32.64]	0.09 [0.01, 0.72]	2.35 [-10.21, 8.00]	0.02 [-0.65, 0.65]	0	5

Microstate ID of Deprotonated State (A)	Microstate ID of Protonated State (HA)	Molecule ID	pKa (exp)	pKa SEM (exp)	pKa ID	Microstate identification source
		SM07	6.08	0.01	SM07_pKa1	NMR measurement
		SM14	5.3	0.01	SM14_pKa2	NMR measurement
		SM14	2.58	0.01	SM14_pKa1	NMR measurement
		SM02	5.03	0.01	SM02_pKa1	Estimated based on SM07 NMR measurement
		SM04	6.02	0.01	SM04_pKa1	Estimated based on SM07 NMR measurement
		SM09	5.37	0.01	SM09_pKa1	Estimated based on SM07 NMR measurement
		SM12	5.28	0.01	SM12_pKa1	Estimated based on SM07 NMR measurement
		SM13	5.77	0.01	SM13_pKa1	Estimated based on SM07 NMR measurement
		SM15	8.94	0.01	SM15_pKa2	Estimated based on SM14 NMR measurement
		SM15	4.7	0.01	SM15_pKa1	Estimated based on SM14 NMR measurement

Figure S1. Dominant microstates of 8 molecules were determined based on NMR measurements. Dominant microstate sequence of 6 derivatives were determined taking SM07 and SM14 as reference. Matched experimental pK_a values were determined by spectrophotometric pK_a measurements [7]. A CSV version of this table can be found in SAMPL6-supplementary-documents.tar.gz.

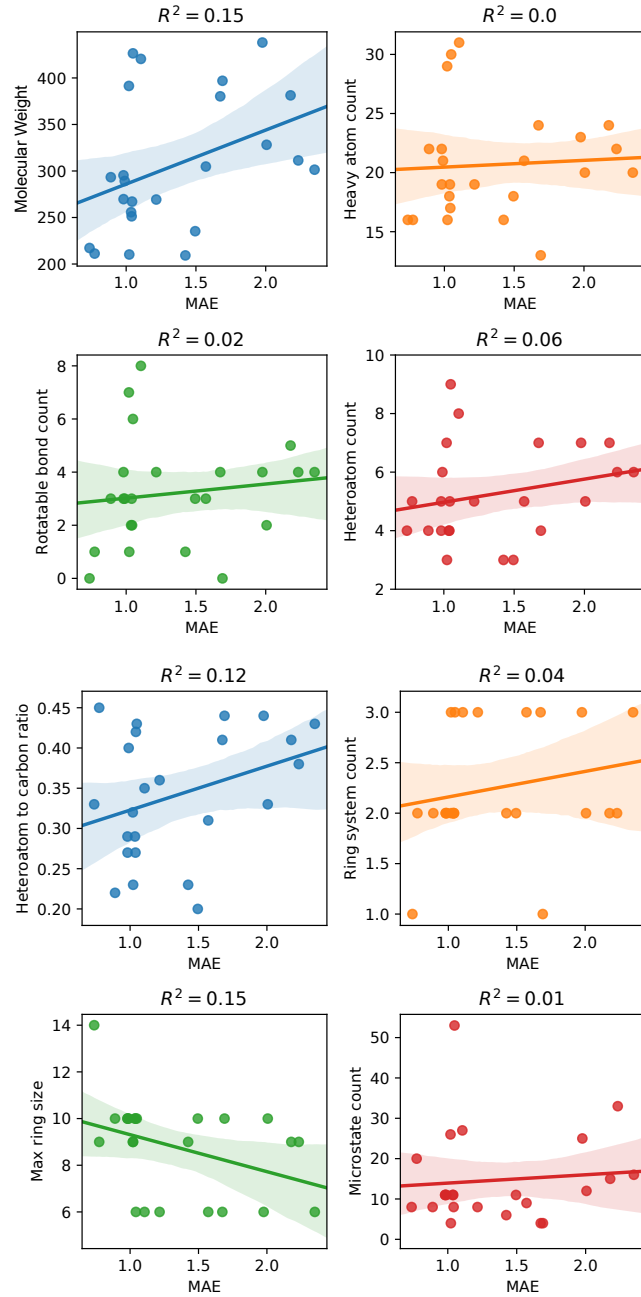


Figure S2. MAE of macroscopic pK_a predictions of each molecule did not show any significant correlation with any molecular descriptor.
 Plots show regression lines, 96% confidence intervals of the regression lines, and R^2 . The following molecular descriptors were calculated using OpenEye OEMolProp Toolkit [35].

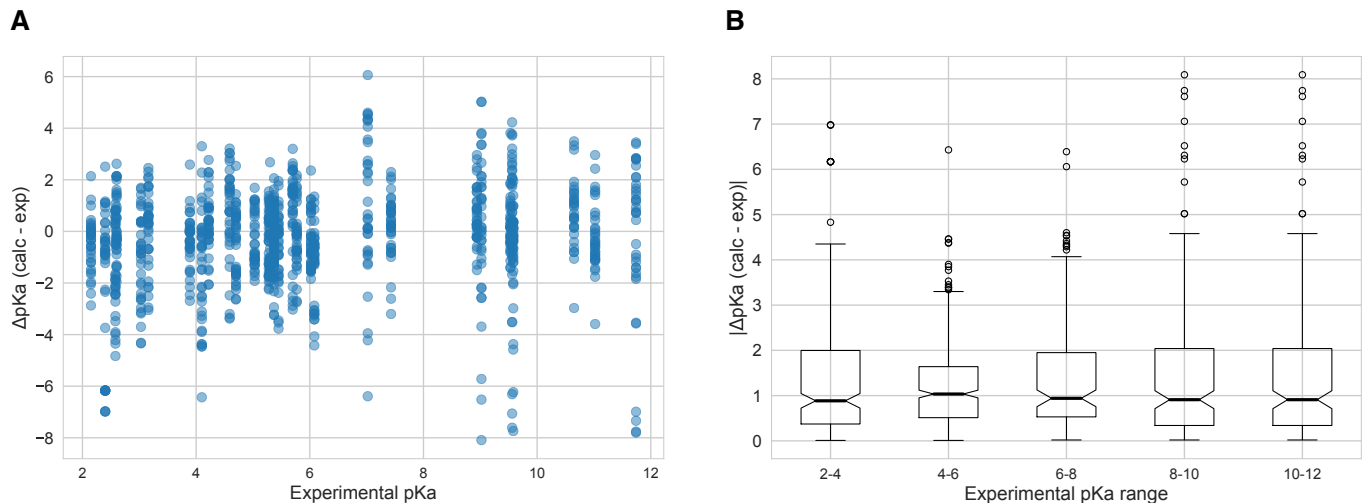


Figure S3. The value of macroscopic pK_a s was not a factor affecting prediction error seen in SAMPL6 Challenge according to the analysis with Hungarian matching. There was not clear trend between pK_a prediction error and the true pK_a error. Very high and very low pK_a values have similar inaccuracy compared to pK_a values close to 7. **A** Scatter plot of macroscopic pK_a prediction error calculated with Hungarian matching vs. experimental pK_a value **B** Box plot of absolute error of macroscopic pK_a predictions binned into 2 pK_a unit intervals of experimental pK_a .

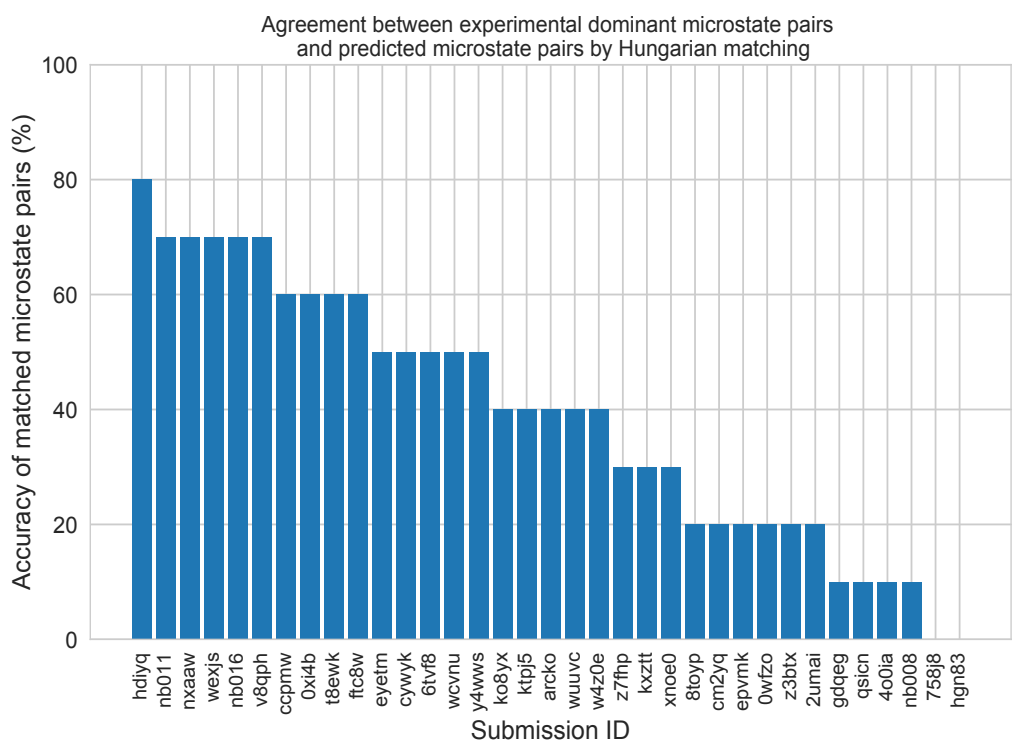


Figure S4. There was low agreement between experimental dominant microstate pairs and the predicted microstate pairs selected by Hungarian algorithm for microscopic pK_a predictions. This analysis could only be performed for 8 molecules with NMR data. Hungarian matching algorithm which matches predicted and experimental values considering only the closeness of the numerical value of pK_a and it often leads to predicted pK_a matches that described a different microstates pair than the experimentally observed dominant microstates..